SIAM J. MATH. ANAL.
Vol. 47, No. 1, pp. 347–380

COMPETITIVE GEOMETRIC EVOLUTION OF AMPHIPHILIC INTERFACES*

SHIBIN DAI† AND KEITH PROMISLOW‡

Abstract. We derive the curvature driven flow of closed-loop pore structures which arise in quasi-stationary states in the H^{-1} gradient flow of the weakly functionalized Cahn–Hilliard free energy which models amphiphilic mixtures. We extend this result to a sharp-interface reduction for the competitive evolution of disjoint collections of bilayer interfaces and closed-loop pores. In particular, for a mixture of spherical bilayers and circular closed pores we explicitly identify two regimes: one in which spherical bilayers extinguish and the circular pores arrive at a common radius, and a complimentary regime in which spherical bilayers of differing radii stably coexist with common-radius, closed-loop, circular pores.

Key words. geometric evolution, functionalized Cahn–Hilliard energy, amphiphilic interface, network formation

AMS subject classifications. 35B40, 35Q74, 35Q92

DOI. 10.1137/130941432

1. Introduction.

Amphiphilic molecules, commonly used as surfactants, possess a hydrophilic and a hydrophobic moiety; when mixed with a suitable solvent the amphiphilic molecules form molecular-width bilayer interfaces and pore structures which interpenetrate the bulk regions of the solvent phase. The amphiphilic nature of the surfactant phase drives interfacial dynamics that are fundamentally different from those observed in mixtures of mutually nonwetting phases. Indeed, the surfactant phase seeks to maximize the interface between hydrophilic groups and solvent, subject to the constraint imposed by available surfactant volume.

In energy conversion materials, such as polymer electrolyte membranes, hydrophilic head groups are tethered to spatially extended hydrophobic polymers, forming an amphiphilic matrix which imbibes solvent, forming counter-ion conducting networks of solvent-filled pores with dominant length-scales ranging from one to four nanometers and solvent accessible surface areas as large as 1000m^2 per gram of material; see [26], [33], [34], and [36]. In this context the solvent is the scarce minority phase, whose volume is restricted by the elastic nature of the polymer electrolyte matrix which resists swelling.

In a biological setting amphiphilic materials include lipids, small biphasic molecules with a polar head group which attracts a hydration sphere of solvent molecules and a "greasy" or "hydrophobic" tail which mixes poorly with solvent. The hydrophilic groups agglomerate with the polar head groups pointing outward so as to interact with the solvent, while the hydrophobic tails lie in a solvent-excluded region. The classic morphology is the bilayer membrane, in which two sheets of lipids align along

*Received by the editors October 16, 2013; accepted for publication (in revised form) November 17, 2014; published electronically January 8, 2015.
http://www.siam.org/journals/sima/47-1/94143.html
†Department of Mathematical Sciences, New Mexico State University, Las Cruces, NM 88003 (sdai@nmsu.edu). The research of this author was supported by the National Science Foundation under grants DMS 093468 and DMS 1411438.
‡Department of Mathematics, Michigan State University, East Lansing, MI 48824 (kpromisl@math.msu.edu). The research of this author was supported by the National Science Foundation under grants DMS 0708804, DMS 093468, and DMS 1125231.

a codimension one hypersurface. When the center-line hypersurface is closed, the resulting structure is called a liposome or vesicle. However, the lipids can also assemble into cylindrical pore-like structures or into spherical micelles with the tails filling the interior.

In recent work, Budin and Szostak [3] investigated the dynamics and division of primitive cellular membranes, comprised primarily of single-chain lipids. They describe the so-called *phospholipid war* in which cells with higher concentrations of phospholipids are more successful in attracting and retaining lipids from the ambient environment. They propose that the resulting selective advantage would drive cells to maximize their phospholipid content, leading them to more closely resemble modern cellular membranes. They also propose a route for cell division in primitive cells via the bifurcation of spherical bilayers (liposomes) into cylindrical pores, which they induce by varying the concentration of free lipids within the solvent phase. Similar budding bifurcations in amphiphilic diblock copolymers are obtained by varying surfactant concentrations; see Figure 1 of [40]. Motivated in part by these experiments, we derive a curvature driven sharp-interface flow for closed cylindrical pores under the weakly functionalized Cahn–Hilliard (FCH) gradient flow and investigate the *competitive* geometric evolution of coexisting liposomes (closed bilayers) with closed cylindrical pores. Our central result describes the role that the "background" or "far-field" value of the surfactant phase residing within the dominant phase has on the competitive evolution of distinct morphologies, particularly bilayer and pore structures.

1.1. Description of the functionalized Cahn–Hilliard free energy. The classical Cahn–Hilliard free energy [4] assigns energy to binary mixtures over a domain $\Omega \subset \mathbb{R}^3$ in terms of the volume fraction $u \in H^1(\Omega)$. Scaling length by $\varepsilon \ll 1$, which describes the typical width of an interfacial thickness, they consider a free energy density $f = f(u, \varepsilon^2|\nabla u|^2, \varepsilon^2 \Delta u)$ as a function of the spatially isotropic differential operators. Expanding f to first order in the differential terms,

$$f(u, \varepsilon^2|\nabla u|^2, \varepsilon^2 \Delta u) = f(u, 0, 0) + A(u)\varepsilon^2|\nabla u|^2 + B(u)\varepsilon^2 \Delta u, \tag{1.1}$$

Cahn and Hilliard obtained their free energy by integrating over the spatial domain,

$$\mathcal{E}(u) = \int_\Omega f(u, 0, 0) + A(u)\varepsilon^2|\nabla u|^2 + B(u)\varepsilon^2 \Delta u \, dx. \tag{1.2}$$

Assuming periodic boundary conditions, integration by parts on the B term yields the more familiar formulation

$$\mathcal{E}(u) = \int_\Omega \frac{\varepsilon^2}{2}|\nabla u|^2 + W(u) \, dx, \tag{1.3}$$

where we have introduced $W(u) := f(u, 0, 0)$ and for simplicity we have set $A(u) - B'(u)$ equal to $\frac{1}{2}$. The mixing potential $W : \mathbb{R} \mapsto \mathbb{R}$ describes the compatibility of the two phases and is typically assumed to be of double-well type with two successive local minima at $b_- < b_+$ with *unequal* depths $W(b_-) = 0 > W(b_+)$ and a transverse intermediate zero at $u_m \in (b_-, b_+)$. Moreover, the minima are assumed to be nondegenerate, with $\alpha_\pm := W''(b_\pm) > 0$.

The Cahn–Hilliard free energy is viewed as a model for mutually immiscible binary mixtures, and its minimizers and gradient flow describe coarsening processes. However, in what follows we are more interested in its nonminimizing critical points

which are found among zeros of the $L^2(\Omega)$ variational derivative of the Cahn–Hilliard energy

$$\frac{\delta \mathcal{E}}{\delta u}(u) := -\varepsilon^2 \Delta u + W'(u) = 0. \tag{1.4}$$

When subject to a total mass constraint

$$\int_\Omega u \, dx = M \tag{1.5}$$

for a prescribed $M \in \mathbb{R}$, the local minimizers of the Cahn–Hilliard free energy include single-layer interfaces, U_s, which separate bulk phases of $u = b_-$ from $u = b_+$ across an order of ε width interface. At leading order the single-layer interface solves the one-dimensional equilibrium equation

$$\partial_z^2 U_s = W'(U_s) + \lambda, \tag{1.6}$$

where z is the ε-scaled distance to the midpoint of the interface and the Lagrange multiplier λ, dual to the mass constraint, takes the critical value for which (1.6) supports a heteroclinic connection. However, the Cahn–Hilliard free energy also supports a wide variety of *saddle point* structures; among these are *bilayer interfaces* U_b which solve

$$\partial_z^2 U_b = W'(U_b), \tag{1.7}$$

subject to the homoclinic conditions, $U = b_-$ at $z = \pm\infty$. These interfaces are also on the order of ε in width but separate two regions of $u = b_-$ by a thin codimension one surface on which u approaches the intermediate zero, $u = u_m \in (b_-, b_+)$, of W. Saddle point structures can also be formed from cylindrically symmetric critical points, which we term *pore solutions*. Indeed, fixing a codimension two interface, Γ_p, which defines the center-line of the pore structure, and introducing R, the ε-scaled radial distance to a Γ_p, the associated pore profile U_p solves the radial version of (1.4),

$$\partial_R^2 U_p + \frac{1}{R}\partial_R U_p = W'(U_p), \tag{1.8}$$

subject to the boundary conditions $\partial_R U_p(0) = 0$ and $U_p \to b_-$ as $R \to \infty$; see Remark 3.2 for a discussion of the existence of U_p. The saddle point structures of $\mathcal{E}$ have qualitative agreement with the morphologies generated by amphiphilic mixtures; see [23], [24], and [40] for experimental examples. In particular, they possess a very large ratio of surface area to volume of minority phase. However, the large surface area saddle point structures are wildly unstable under gradient flows of the Cahn–Hilliard energy.

To model amphiphilic mixtures, such as emulsions formed by adding a minority fraction of an oil and soap mixture to water, small-angle X-ray scattering (SAXS) data motivated several authors (see [37] and [18]) to include a higher-order term in the usual Cahn–Hilliard expansion of a binary mixture. Specifically, these authors truncated the Cahn–Hilliard expansion at the second order in $\varepsilon^2 \Delta u$, obtaining

$$\mathcal{F}(u) := \int_\Omega f(u,0,0) + \varepsilon^2 A(u)|\nabla u|^2 + \varepsilon^2 B(u)\Delta u + \overbrace{C(u)}^{\geq 0}(\varepsilon^2 \Delta u)^2 \, dx, \tag{1.9}$$

and related the sign of $A(u) - B'(u)$ to the mixture's amphiphilicity. However, in this formulation the system is unwieldy for a systematic study. It is preferable to identify a normal form from which new structures can be identified as they bifurcate from simpler ones. To this end, we shift all the differential terms to powers of Laplacians; specifically, we replace $A(u)\nabla u$ with $\nabla\overline{A}(u)$, where $\overline{A}$ is the primitive of A, and integrate by parts. The result is a free energy in u and in $\varepsilon^2\Delta u$ up to quadratic terms. Setting $C(u) \equiv \frac{1}{2}$ and completing the square in $\varepsilon^2\Delta u$ results in the general form

$$\mathcal{F}(u) = \int_\Omega \frac{1}{2}\left(\varepsilon^2\Delta u - W'(u)\right)^2 + \delta P(u)\, dx, \tag{1.10}$$

where we have suggestively rewritten the potential inside the square as W', to draw an analogy to the variational derivative of a Cahn–Hilliard type energy (1.4), and scaled the potential, P, outside of the square by $\delta \in \mathbb{R}$. The form (1.10) is a relatively generic reformulation of (1.9). To arrive at our normal form we make two nongeneric assumptions; the first is that the potential $W(u)$ is of double-well type, as for the usual Cahn–Hilliard energy. In this context we associate $u = b_-$ to the bulk solvent phase, with the value of $u - b_- > 0$ being proportional to the density of the amphiphilic phase. The second assumption is that $\delta \ll 1$; that is, the free energy is close to being a perfect square. This assumption allows us to perturb off of the highly degenerate case of the perfect square ($\delta = 0$), for which the global minimizers of $\mathcal{F}$ are precisely the *critical points* of an associated Cahn–Hilliard energy. Indeed, a variant of this case was proposed as a target for Γ-convergence analysis by De Giorgi; see [32].

The weakly FCH free energy, proposed in [16], corresponds to the distinguished limit $\delta = \varepsilon^2$, and a particular choice for the perturbing potential, P,

$$\mathcal{F}_{\mathrm{CH}}(u) := \int_\Omega \frac{1}{2}\left(\varepsilon^2\Delta u - W'(u)\right)^2 - \varepsilon^2\left(\frac{\varepsilon^2\eta_1}{2}|\nabla u|^2 + \eta_2 W(u)\right) dx. \tag{1.11}$$

The functionalization terms, parameterized by $\eta_1 > 0$ and $\eta_2 \in \mathbb{R}$, are analogous to the surface and volume energies typical of models of charged solutes in confined domains; see [35] and particularly equation (67) of [1]. The minus sign in front of η_1 is of considerable significance; it incorporates the propensity of the amphiphilic surfactant phase to drive the creation of interface. Indeed, experimental tuning of solvent quality shows that morphological instability in amphiphilic mixtures is associated to (small) negative values of surface tension [40], [41]. Note that the form $\frac{\varepsilon^2}{2}\eta_1|\nabla u|^2$ can be rewritten as a pure potential $2\eta_1 u W'(u)$ after an integration by parts on $|\nabla u|^2$ and absorbing the resulting $-\varepsilon^2\eta_1 u\Delta u$ as an $O(\varepsilon^2)$ perturbation to $W'(u)$ within the quadratic term. However, the form $-\eta_1|\nabla u|^2 < 0$ is more clearly sign-definite and localized on interfaces. This term is associated to single layers of surfactant molecules, whose growth lowers overall system energy; however, the effect is *perturbative*, and unrestricted growth is arrested by the penalty nature of the square term which keeps u close to the critical points of $\mathcal{E}_{\mathrm{CH}}$.

The dominant term in the FCH free energy, referred to loosely as the Willmore contribution, is the square of the $L^2(\Omega)$ variational derivative of a Cahn–Hilliard type energy in the form of (1.4). The weak functionalization, taken here and in Γ-limit scalings, considers the $\delta = \varepsilon^2$ distinguished limit in which the functionalization terms balance with the square of the $O(\varepsilon)$ residuals, the Willmore terms, appearing in $\frac{\delta\mathcal{E}}{\delta u}$. As we shall see, the weak scaling leads to morphological competition on the $O(\varepsilon^{-2})$ time scale which is nonlinear in curvature. The strong functionalization, considered

in [11], considers the distinguished limit $\delta = \varepsilon$, in which the functionalization terms dominate the Willmore residual, leading to a morphological competition on the $O(\varepsilon^{-1})$ time scale which is linear in curvature.

For $\eta_1 > 0$, the first functionalization term assigns lower free energy to critical point structures of the Cahn–Hilliard free energy with large surface area. As a model of amphiphilic mixtures, this corresponds to the energetic preference for the surfactant phase to spread out in a thin interfacial layer whose extent is constrained by the volume of surfactant and by their molecular width [17]. Within the framework of the FCH free energy, the molecular width is described by the width of the bilayer, U_b, and pore, U_p, profiles. The second perturbative term, $\eta_2 W(u)$, incorporates pressure jumps between solvent and surfactant phases, and the choice of W as the pressure jump potential is predicated by the fact that its bilayer contribution $W(\Phi_b) > 0$ is positive, while its pore contribution, $W(\Phi_p)$, averages spatially to zero.

Single-layer interfaces have been employed to describe a wide range of physical phenomena. Higher-order free energies, similar to the FCH with the significant exception that $\eta_1 < 0$ and the mixing well W is untitled, have been proposed; see [27] and [38]. Indeed, the De Giorgi conjecture, which concerns the Γ-limit of the FCH energy for $\eta_1 < 0$ with an untilted well, has been established [32]. Extensions of these models to address deformations of elastic vesicles subject to volume constraints [13] and multicomponent models which incorporate a variable intrinsic curvature have been investigated [28]. However, the single-layer interface forms the essential underpinning of each of these models. For amphiphilic materials with $\eta_1 > 0$ the FCH energy landscape is fundamentally different. Indeed, for fixed $\varepsilon > 0$ the FCH energy is bounded below and has global minimizers (see [31]); *however*, for $\eta_1 > 0$ the lower bound tends to $-\infty$ as $\varepsilon \to 0^+$ for fixed volume fraction. A Γ-limit analysis of the FCH will require new ideas, particularly since defect structures, such as end-caps and junctions, may form spatially dense sets as $\varepsilon \to 0^+$.

1.2. Main results. This paper addresses the competitive evolution of bilayer and pore structures under the FCH equation: the H^{-1} gradient flow of the FCH energy

$$u_t = \Delta \overbrace{\left\{\left(-\varepsilon^2\Delta + W''(u) - \varepsilon^2\eta_1\right)\left(-\varepsilon^2\Delta u + W'(u)\right) + \varepsilon^2(\eta_1 - \eta_2)W'(u)\right\}}^{\mu := \frac{\delta \mathcal{F}}{\delta u}}, \tag{1.12}$$

over a function space $H^6_N(\Omega)$, where the N subscript denotes zero-flux boundary conditions, such as periodic or homogeneous Neumann ($\vec{n}\cdot\nabla u = \vec{n}\cdot\nabla\Delta u = \vec{n}\cdot\nabla\mu = 0$ on $\partial\Omega$) boundary conditions. Here we define the chemical potential μ as

$$\mu := \frac{\delta \mathcal{F}}{\delta u} = \left(-\varepsilon^2\Delta + W''(u) - \varepsilon^2\eta_1\right)\left(-\varepsilon^2\Delta u + W'(u)\right) + \varepsilon^2(\eta_1 - \eta_2)W'(u).$$

We consider the evolution of a disjoint family of codimension one bilayer morphologies, with center-line hypersurface $\Gamma_b \subset \mathbb{R}^3$ together with a disjoint family of codimension two pore morphologies, with center-curve $\Gamma_p \subset \mathbb{R}^3$, which are far from self-intersection, or from intersecting each other, as measured in the ε-scaled distance. A key result is that, away from the interfaces, the chemical potential is spatially constant,

$$\mu(t) := \mu_0 + \varepsilon\mu_1(t) + \varepsilon^2\mu_2(t) + O(\varepsilon^3),$$

and moreover the competitive evolution of the interfaces is mediated through this far-field value of the chemical potential, which we show is proportional to the density of surfactant (lipids) in the bulk (solvent) phase.

In [10] we derived the evolution of a disjoint family $\Gamma_b = \cup_{i=1}^{N_b} \Gamma_{b,i}$ of closed, codimension one bilayer interfaces in $\mathbb{R}^n$ in terms of its normal velocity. A geometric normal velocity specifics the motion of an interface in terms of its intrinsic quantities, generically its curvatures. Moreover, the form of the geometric bilayer normal velocity differs on distinct time scales. On the $t_1 = \varepsilon t$ time scale the result is a classic curvature driven flow with a velocity proportional to the chemical potential, μ_1, which in turn decays exponentially in time, yielding a quenched curvature driven flow. However, in this work we focus on the $t_2 := \varepsilon^2 t$ time scale, for which we derived a Willmore-type geometric normal velocity prescribed by

$$V_b = \frac{\sigma_b}{m_b}\left(\Delta_s + K - \frac{1}{2}H^2 + \frac{\eta_1 + \eta_2}{2} + \lambda_b \mu_2\right) H, \tag{1.13}$$

where, for $n = 3$, the total and quadratic curvatures $H = k_1 + k_2$ and $K = k_1^2 + k_2^2$ are defined in terms of the principle curvatures k_i, $i = 1, 2$, of Γ_b. The operator Δ_s is the Laplace–Beltrami operator associated to Γ_b, and

$$m_b := \int_{\mathbb{R}} \hat{U}_b(z)\, dz, \qquad \lambda_b := \frac{2m_b}{\int_{\mathbb{R}} |\hat{U}_b'|^2\, dz}, \qquad \sigma_b := \frac{m_b \int_{\mathbb{R}} |\hat{U}_b'|^2\, dz}{\int_{\mathbb{R}} |\hat{U}_b|^2\, dz} \tag{1.14}$$

are positive constants determined solely by the double-well potential W in the FCH energy through the shifted bilayer profile $\hat{U}_b := U_b - b_-$, which describes the amphiphilic volume above the reference value b_- in terms of the bilayer profile defined in (1.7). In particular, m_b denotes the mass of surfactant per unit area of bilayer. For single-layer interfaces, the interface evolution is governed by a Mullins–Sekerka flow, as in [29]. For bilayers the Mullins–Sekerka problem is trivial, leading to a spatially constant chemical potential, $\mu_2 = \mu_2(t_2)$, whose value is determined by conservation of total mass. The end result is an *interfacial-area preserving* Willmore flow. Indeed, at leading order the mass of amphiphile per unit surface area of bilayer is fixed, so the evolution of quasi-equilibrated bilayers under (1.13) cannot change the total surface area; it is at the second order in ε that the value of μ_2 is determined so that the total mass is preserved.

In this work, we first establish the geometric evolution of a collection of disjoint closed-loop pores in $\mathbb{R}^3$, characterized by a collection of codimension two interfaces $\Gamma_p = \cup_{i=1}^{N_p} \Gamma_{p,i}$. Subsequently we show that the geometric evolution of coexisting pore and bilayer structures is mediated through the common value of the far-field chemical potential, $\mu_2 = \mu_2(t_2)$, which is proportional to the ambient level of surfactant phase in the solvent domain. Our results are formal, and in particular we assume that the bilayer and pore profiles are stable. It is shown in [20] that the sole mechanisms for linear instability of a bilayer interface are either through the meander instability, which relates to motion of the underlying codimension one interface Γ, or through high-frequency, in-plane modulations of the bilayer width, called a pearling instability. Detailed conditions under which the pearling instability are manifest have been determined for both the strong and weak functionalization [11, 12]. We assume that the underlying pore structures are stable up to the meander motion of the underlying manifold Γ_p, whose evolution we address through a multiscale reduction resulting in distinct geometric flows on the $t_1 = \varepsilon^{-1} t$ and $t_2 = \varepsilon^{-2} t_2$ time scales. Indeed, on the t_1 time scale we recover a quenched mean-curvature flow for pores, governed by the coupled system (5.2) and (5.41). While we derive results on a variety of time scales, we emphasize those on the t_2 time scale, which we couple to results for the bilayers. Placing these results in the proper context requires the following definition.

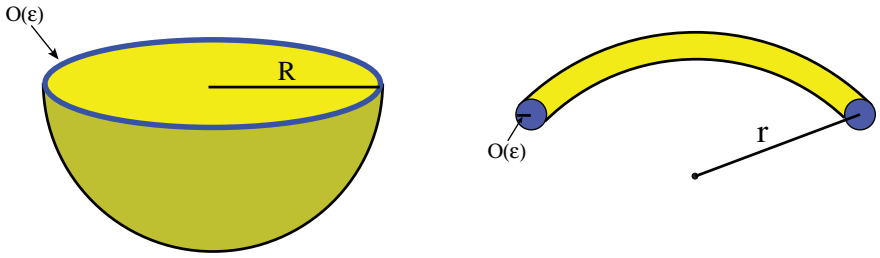

FIG. 1. *Bottom half of a spherical bilayer of radius R and an arc-length of a closed circular pore of radius $r > 0$. The structures are cut to show the inner width, which is $O(\varepsilon)$. The surfactant phase is colored blue, while the surface is yellow.*

DEFINITION 1.1. *We say that the interfaces Γ_b and Γ_p are at* quasi equilbrium *if all transient dynamics are at equilibrium for the time scales that are as fast as, or faster than, $t_1 = t/\varepsilon$. Equivalently, the spatially constant chemical potential satisfies $\mu_0 = \mu_1 = 0$; see* (4.1), (4.30), (5.2), *and* (5.41) *as well as* (1.7)–(1.8) *of* [10].

Our main results concern the evolution of disjoint collections of pores and bilayers at quasi equilbrium.

PRINCIPLE RESULT 1.1. *We assume that the pore and bilayer morphologies are stable with respect to the pearling instabilities and that Assumption* 3.3 *holds for fixed $\Omega \subset \mathbb{R}^3$ with $|\Omega|$ independent of $\varepsilon > 0$ and a collection of well-separated, quasi-equilibrium bilayer and pore structures, with center interface $\Gamma_b = \cup_{i=1}^{N_b} \Gamma_{b,i}$ and center line $\Gamma_p = \cup_{i=1}^{N_p} \Gamma_{p,i}$, whose total masses $m_b|\Gamma_b|$ and $\varepsilon m_p|\Gamma_p|$ are both order of* 1 *with respect to ε. Then under the weak FCH gradient flow* (1.12), *the evolution of the underlying center structures is given by the bilayer normal velocity* (1.13) *coupled to the vector-valued pore normal velocity*

$$\mathbf{V}_p = -\frac{\sigma_p}{m_p}\left(\partial_s^2 + \frac{1}{4}|\vec{\kappa}|^2 + \eta_1 + \lambda_p\mu_2\right)\vec{\kappa}, \tag{1.15}$$

where $m_p := 2\pi S_1$, the mass per unit length of pore, and the positive constants $\sigma_p := 2\pi S_1 S_4/S_2$ and $\lambda_p := 2S_1/S_4$ depend upon the double-well, W, through the pore profile, U_p, defined in (1.8), *via the relations* (4.23) *and* (6.24). *The vector-valued pore normal velocity $\mathbf{V}_p$ and vector pore curvature $\vec{\kappa} = (\kappa_1, \kappa_2)^t$ are taken in the coordinate system of Lemma* 2.2; *see also* (6.34). *The coupling between the bilayer and pore normal velocities is through the spatially constant value of $\mu_2 = \mu_2(t_2)$, which is determined from the mass constraint*

$$0 = m_b\frac{d}{dt}|\Gamma_b| + m_p\varepsilon\frac{d}{dt}|\Gamma_p| = m_b\int_{\Gamma_b} V_b(S)H(S)\,dS - m_p\varepsilon\int_{\Gamma_p}\mathbf{V}_p(s)\cdot\vec{\kappa}(s)\,ds. \tag{1.16}$$

To illuminate the structure of the coupled evolution we consider the special case of collections of $N_b \in \mathbb{N}_+$ spherical bilayer structures with radii $R_i(t)$ for $i = 1, \ldots, N_b$, and $N_p \in \mathbb{N}_+$ closed, circular pores of radii r_i for $i = 1, \ldots, N_p$; see Figure 1. To be consistent with a total surfactant phase which is $O(\varepsilon)$, we assume that each radius is $O(1)$, and $N_b = O(1)$ while $N_p = O(\varepsilon^{-1})$; see Figure 1. Moreover, we assume that the spherical and circular symmetry persists on the t_2 time scale.

PRINCIPLE RESULT 1.2. *If, in addition to the assumptions of Principle Result* 1.1, *we consider a collection of spherical bilayers and circular pores, then the coupled*

evolution, (1.13)*,* (1.15)*, and* (1.16)*, reduces to a system of ODEs for the radii given by* (7.10)–(7.11) *coupled through* (7.12)*. In particular, if the bifurcation parameter,*

$$\nu := (\lambda_p - 2\lambda_b)\eta_1 + \lambda_p \eta_2, \tag{1.17}$$

satisfies $\nu < 0$*, then the circular pores will grow until the spherical bilayers extinguish, while if* $\nu > 0$*, then there are configurations of coexisting circular pores with common radii and spherical bilayers with arbitrary radii which are asymptotically stable with respect to perturbations of the radii.*

In section 2 we establish the coordinate system for the codimension two structures and introduce the near- and far-field expansions for the chemical potentials and pore profile. In section 3 we address the relaxation of the FCH equation for initial data in the neighborhood of a pore structure, on the fast $T_2 = t/\varepsilon^2$ time scale. In section 4 we address the $t = O(1)$ time scale, deriving a free surface problem which possesses spatially constant outer solutions. In section 5 we address the $t_1 = \varepsilon t$ time scale, deriving a coupled system, (5.31) and (5.41), for the normal velocity and far-field chemical potential. The curvature driven flow is quenched by the chemical potential, whose expression of mass conservation serves to arrest the flow, driving it to equilibria. In section 6 we analyze the $t_2 = \varepsilon^2 t$ time scale, deriving the length-preserving Willmoresque flow (6.45) for well-separated, closed-loop pores. In section 7 we couple the evolution of the closed-loop pores to that of bilayers derived in [10], yielding Principle Result 1.1. Indeed, since at the order of our analysis the bilayers and pores asymptote to spatially constant far field states, the combined evolution follows by coupling the pore normal velocity, derived in (6.34), and the associated chemical potential evolution, (6.44), to the bilayer normal velocity (1.13) through combined mass constraint derived in (7.7). In the remainder of section 7 the resulting evolution is reduced and analyzed for the special case of spherical bilayers and circularly symmetric pore structures, with the results summarized in Principle Result 1.2.

2. Moving frame, inner expansion, and normal derivatives. We first address the codimension two structures. We consider a smooth, closed curve $\Gamma \subset \mathbb{R}^3$ parameterized by ϕ,

$$\Gamma(t) = \left\{ \phi(s,t) : [0, L(t)] \times [0,T] \mapsto \mathbb{R}^3 \middle| \quad \phi(0,t) = \phi(L(t),t)) \right\}, \tag{2.1}$$

where s denotes arc-length and $L = L(t)$ is the total curve length. At a given point on Γ, the unit tangent vector $\mathbf{T}$, the principal normal vector $\mathbf{N}$, and the binormal vector $\mathbf{B}$, defined by

$$\mathbf{T} = \frac{\partial \phi}{\partial s}, \quad \mathbf{N} = \left\| \frac{\partial \mathbf{T}}{\partial s} \right\|^{-1} \frac{\partial \mathbf{T}}{\partial s}, \quad \mathbf{B} = \mathbf{T} \times \mathbf{N}, \tag{2.2}$$

form the Frenet–Serret frame. For fixed t the vectors are coupled via the curvature κ and torsion τ of the curve. The Frenet–Serret formulas are

$$\frac{\partial \mathbf{T}}{\partial s} = \kappa \mathbf{N}, \tag{2.3}$$

$$\frac{\partial \mathbf{N}}{\partial s} = -\kappa \mathbf{T} + \tau \mathbf{B}, \tag{2.4}$$

$$\frac{\partial \mathbf{B}}{\partial s} = -\tau \mathbf{N}. \tag{2.5}$$

The $\{\mathbf{T}, \mathbf{N}, \mathbf{B}\}$ coordinate system is not convenient for our calculations due to the asymmetry of the roles played by $\mathbf{N}$ and $\mathbf{B}$. To circumvent this, we define a new coordinate system, $\{\mathbf{T}, \mathbf{N}^1, \mathbf{N}^2\}$, such that at each point $\phi(s,t)$ on the curve $\Gamma(t)$ the vectors $\{\mathbf{N}^1, \mathbf{N}^2\}$ form an orthonormal basis for the normal plane and

$$\frac{\partial \mathbf{N}^i}{\partial s} = -\kappa_i \mathbf{T}, \quad i = 1, 2, \tag{2.6}$$

where $\vec{\kappa}(s,t) := (\kappa_1, \kappa_2)^t$ is the normal curvature vector with respect to $\{\mathbf{N}^1, \mathbf{N}^2\}$. The same orthonormal basis has been used by Calini and Ivey for the study of the motion of thin vortex filaments in an ideal fluid [5]. Here we include an existence result in the general setting.

LEMMA 2.1. *Let $M \in \mathbb{R}^{2\times 2}$ satisfy the differential equation*

$$\frac{d}{ds} M(s) = \begin{pmatrix} 0 & \tau(s) \\ -\tau(s) & 0 \end{pmatrix} M(s), \tag{2.7}$$

subject to initial data $M(0) = M_0$. If M_0 is orthonormal, then so is M, and the vectors $\{\mathbf{N}^1, \mathbf{N}^2\}$ defined by

$$\big(\mathbf{N}^1(s), \mathbf{N}^2(s)\big) := \big(\mathbf{N}(s), \mathbf{B}(s)\big) M(s) \tag{2.8}$$

form an orthonormal basis for the normal plane and satisfy (2.6) *with*

$$\kappa_i(s) = M_{1i}(s)\kappa(s) \tag{2.9}$$

for $i = 1, 2$.

Proof. Let the initial data M_0 be an orthonormal matrix, and let M be the corresponding solution of (2.7). We observe that $\frac{d}{ds}(M^t M) = 0$, and since $M_0^t M_0 = I$, we have $M^t M = I$ for all s; that is, $M(s)$ is orthonormal. The vectors $\{\mathbf{N}^1, \mathbf{N}^2\}$ defined by (2.8) are orthonormal and lie in the normal plane to Γ at s; hence they span the plane. In addition, taking ∂_s of (2.8) and using the Frenet relations (2.3)–(2.5) and (2.6), we find

$$\begin{aligned} \frac{\partial \mathbf{N}^i}{\partial s} &= M_{1i}' \mathbf{N} + M_{2i}' \mathbf{B} + M_{1i} \frac{\partial \mathbf{N}}{\partial s} + M_{2i} \frac{\partial \mathbf{B}}{\partial s} \\ &= \tau M_{2i} \mathbf{N} - \tau M_{1i} \mathbf{B} + M_{1i} (-\kappa \mathbf{T} + \tau \mathbf{B}) - M_{2i} \tau \mathbf{N} = -\kappa_i \mathbf{T}, \end{aligned}$$

which establishes (2.6) for κ_i defined in (2.9). ∎

We define the normal velocity $\mathbf{V} = (V_1, V_2)^t$ of the point $\phi(s,t)$ on $\Gamma(t)$ via

$$V_i := \mathbf{N}^i \cdot \frac{\partial \phi}{\partial t}(s,t) \tag{2.10}$$

for $i = 1, 2$. The following lemma demonstrates the utility of the $\{\mathbf{T}, \mathbf{N}^1, \mathbf{N}^2\}$ coordinates.

LEMMA 2.2. *The $\{\mathbf{T}, \mathbf{N}^1, \mathbf{N}^2\}$ coordinate system satisfies*

$$\frac{\partial \mathbf{T}}{\partial s} = \kappa_1 \mathbf{N}^1 + \kappa_2 \mathbf{N}^2, \tag{2.11}$$

while the curve length evolves according to

$$\frac{d|\Gamma|}{dt} = -\int_\Gamma \mathbf{V} \cdot \vec{\kappa}\, ds. \tag{2.12}$$

Proof. Taking ∂_s of $\mathbf{T}\cdot\mathbf{T}=1$, we see that $\frac{\partial\mathbf{T}}{\partial s}\cdot\mathbf{T}=0$, and hence $\frac{\partial\mathbf{T}}{\partial s}=a_1(s)\mathbf{N}^1+a_2(s)\mathbf{N}^2$ for some functions $a_1(s)$, $a_2(s)$. Moreover, taking ∂_s of $0=\mathbf{T}\cdot\mathbf{N}^i$, we arrive at the relation

$$0=\frac{\partial\mathbf{T}}{\partial s}\cdot\mathbf{N}^i+\mathbf{T}\cdot\frac{\partial\mathbf{N}^i}{\partial s}=a_i(s)-\kappa_i, \tag{2.13}$$

and hence $a_i=\kappa_i$.

To calculate the change in curve length it is convenient to parameterize the family of curves $\{\Gamma(t):t_0-\delta<t<t_0+\delta\}$ by a common parameter $\xi\in[a,b]$:

$$\Gamma(t)=\{\gamma(\xi,t):\xi\in[a,b]\}\quad\text{for all } t\in(t_0-\delta,t_0+\delta). \tag{2.14}$$

We take ξ to be the arc-length parameter at $t=t_0$. It follows that

$$|\Gamma(t)|=\int_a^b\left\|\frac{\partial\gamma}{\partial\xi}(\xi,t)\right\|\,d\xi,$$

and taking the time derivative we find

$$\begin{aligned}\frac{d|\Gamma|}{dt}&=\int_a^b\frac{\partial}{\partial t}\left\|\frac{\partial\gamma}{\partial\xi}(\xi,t)\right\|\,d\xi=\int_a^b\left\|\frac{\partial\gamma}{\partial\xi}(\xi,t)\right\|^{-1}\frac{\partial\gamma}{\partial\xi}\cdot\frac{\partial^2\gamma}{\partial\xi\partial t}\,d\xi\\&=-\int_a^b\frac{\partial}{\partial\xi}\left(\left\|\frac{\partial\gamma}{\partial\xi}(\xi,t)\right\|^{-1}\frac{\partial\gamma}{\partial\xi}\right)\cdot\frac{\partial\gamma}{\partial t}\,d\xi,\end{aligned} \tag{2.15}$$

where the boundary terms canceled in the integration by parts since $\Gamma(t)$ is smooth and closed. Since ξ corresponds to arc-length at $t=t_0$, we have

$$\frac{\partial\gamma}{\partial\xi}(\xi,t_0)=\mathbf{T},\quad\left\|\frac{\partial\gamma}{\partial\xi}(\xi,t_0)\right\|=1, \tag{2.16}$$

and substituting $t=t_0$ into (2.15) yields

$$\begin{aligned}\frac{d|\Gamma|}{dt}(t_0)&=-\int_a^b\frac{\partial\mathbf{T}}{\partial\xi}\cdot\frac{\partial\gamma}{\partial t}\,d\xi=-\int_a^b(\kappa_1\mathbf{N}^1+\kappa_2\mathbf{N}^2)\cdot\frac{\partial\gamma}{\partial t}\,d\xi\\&=-\int_a^b(\kappa_1V_1+\kappa_2V_2)\,d\xi=-\int_\Gamma(\kappa_1V_1+\kappa_2V_2)\,ds.\end{aligned} \tag{2.17}$$

∎

Assuming that Γ is smooth, from the implicit function theorem there is a neighborhood $\Gamma_\ell\subset\mathbb{R}^3$ of Γ such that each $x\in\Gamma_\ell$ can be uniquely represented as

$$x=\phi(s,t)+r_1\mathbf{N}^1(s,t)+r_2\mathbf{N}^2(s,t), \tag{2.18}$$

where $s=s(x,t)$ and $\vec{r}=(r_1(x,t),r_2(x,t))$ are as smooth as γ'. In the rescaled normal coordinates $z=(z_1,z_2)^t:=\varepsilon^{-1}\vec{r}$ we have the following identities.

LEMMA 2.3. *Fix Γ and assume that ℓ is so small that $\|\vec{\kappa}\|_{L^\infty(\Gamma)}\ell<1$. Then on Γ_ℓ, the change of variables $(x,t)\mapsto(s,z,t)$ transforms the Cartesian Laplacian to*

$$\Delta_x=\varepsilon^{-2}\Delta_z-\varepsilon^{-1}\frac{\vec{\kappa}}{1-\varepsilon z\cdot\vec{\kappa}}\cdot\nabla_z+\frac{1}{(1-\varepsilon z\cdot\vec{\kappa})^2}\partial_s^2+\frac{\varepsilon z\cdot\partial_s\vec{\kappa}}{(1-\varepsilon z\cdot\vec{\kappa})^3}\partial_s, \tag{2.19}$$

while the normal velocity $\mathbf{V}$ takes the form

$$V_1=-\varepsilon\frac{\partial z_1}{\partial t}+\varepsilon z_2\mathbf{N}^2\cdot\frac{\partial\mathbf{N}^1}{\partial t}, \tag{2.20}$$

$$V_2 = -\varepsilon \frac{\partial z_2}{\partial t} + \varepsilon z_1 \mathbf{N}^1 \cdot \frac{\partial \mathbf{N}^2}{\partial t}. \tag{2.21}$$

Moreover, the Jacobian associated to the change of variables takes the form

$$J(s,z) = \varepsilon^2 - \varepsilon^3 z \cdot \vec{\kappa}. \tag{2.22}$$

Proof. The relation (2.19) follows from a standard calculation. To obtain the normal velocity expressions we rewrite (2.18) as

$$\varepsilon z_1(x,t) = (x - \phi(s,t)) \cdot \mathbf{N}^1(s,t), \quad \varepsilon z_2(x,t) = (x - \phi(s,t)) \cdot \mathbf{N}^2(s,t). \tag{2.23}$$

Taking ∂_t of the z_1 equation, we find

$$\begin{aligned} \varepsilon \frac{\partial z_1}{\partial t} &= \left(-\frac{\partial \phi}{\partial s}\frac{\partial s}{\partial t} - \frac{\partial \phi}{\partial t} \right) \cdot \mathbf{N}^1 + (x - \phi(s,t)) \cdot \left(\frac{\partial \mathbf{N}^1}{\partial s}\frac{\partial s}{\partial t} + \frac{\partial \mathbf{N}^1}{\partial t} \right) \\ &= \left(-\mathbf{T}\frac{\partial s}{\partial t} - \frac{\partial \phi}{\partial t} \right) \cdot \mathbf{N}^1 + \varepsilon (z_1 \mathbf{N}^1 + z_2 \mathbf{N}^2) \cdot \left(-\kappa_1 \mathbf{T}\frac{\partial s}{\partial t} + \frac{\partial \mathbf{N}^1}{\partial t} \right) \\ &= -\frac{\partial \phi}{\partial t} \cdot \mathbf{N}^1 + \varepsilon z_2 \mathbf{N}^2 \cdot \frac{\partial \mathbf{N}^1}{\partial t}. \end{aligned} \tag{2.24}$$

The relations (2.10) yield (2.20), and the derivation of (2.21) is similar. The Jacobian matrix takes the form

$$\mathbf{J} = \frac{\partial x}{\partial (s, z_1, z_2)} = \big((1 - \varepsilon z_1 \kappa_1 - \varepsilon z_2 \kappa_2)\mathbf{T}, \varepsilon \mathbf{N}^1, \varepsilon \mathbf{N}^2 \big), \tag{2.25}$$

and evaluating the determinant yields (2.22). ∎

Remark 2.4. The terms $z_2 \mathbf{N}^2 \cdot \frac{\partial \mathbf{N}^1}{\partial t}$ and $z_1 \mathbf{N}^1 \cdot \frac{\partial \mathbf{N}^2}{\partial t}$ in (2.20) and (2.21) reflect lower-order contributions to the normal velocity induced by the rotational motion of the curve $\Gamma(t)$.

For notational convenience we introduce

$$\Delta_0 := \frac{\partial^2}{\partial s^2} - (z \cdot \vec{\kappa})\vec{\kappa} \cdot \nabla_z \tag{2.26}$$

and rewrite the Cartesian Laplacian expansion (2.19) in the more compact form

$$\Delta_x = \varepsilon^{-2}\Delta_z - \varepsilon^{-1}\vec{\kappa} \cdot \nabla_z + \Delta_0 + \varepsilon \Delta_1 + O(\varepsilon^2), \tag{2.27}$$

where the precise forms of Δ_1 and the lower-order terms are immaterial for the analysis. Considering a time scale $\tilde{t}$, we have the formal inner expansion of a quantity v,

$$v(x,t) = \tilde{v}(s,z,t) = \tilde{v}_0 + \varepsilon \tilde{v}_1 + \varepsilon^2 \tilde{v}_2 + \varepsilon^3 \tilde{v}_3 + O(\varepsilon^4), \tag{2.28}$$

where $\tilde{v}_i = \tilde{v}_i(s,z,\tilde{t})$. The Cartesian Laplacian of v then admits the inner expansion

$$\begin{aligned} \Delta_x v &= \varepsilon^{-2}\Delta_z \tilde{v} - \varepsilon^{-1}\vec{\kappa} \cdot \nabla_z \tilde{v} + \Delta_0 \tilde{v} + O(\varepsilon) \\ &= \varepsilon^{-2}\Delta_z \tilde{v}_0 + \varepsilon^{-1}\left(\Delta_z \tilde{v}_1 - \vec{\kappa} \cdot \nabla_z \tilde{v}_0\right) + \left(\Delta_z \tilde{v}_2 - \vec{\kappa} \cdot \nabla_z \tilde{v}_1 + \Delta_0 \tilde{v}_0\right) \\ &\quad + \varepsilon\left(\Delta_z \tilde{v}_3 - \vec{\kappa} \cdot \nabla_z \tilde{v}_2 + \Delta_0 \tilde{v}_1 + \Delta_1 \tilde{v}_0\right) + O(\varepsilon^2). \end{aligned} \tag{2.29}$$

To develop an inner expansion for the chemical potential, μ, we substitute the inner expansion (2.28) of u into (1.12), obtaining

$$\begin{aligned}
\mu(x,t) &= \left(-\varepsilon^2\Delta_x + W''(u) - \varepsilon^2\eta_1\right)\left(-\varepsilon^2\Delta_x u + W'(u)\right) + \varepsilon^2(\eta_1-\eta_2)W'(u)\\
&= \Bigg[-\Delta_z + W''(\tilde u_0) + \varepsilon\left(\vec\kappa\cdot\nabla_z + W'''(\tilde u_0)\tilde u_1\right)\\
&\quad + \varepsilon^2\left(-\Delta_0 + W'''(\tilde u_0)\tilde u_2 + W^{(4)}(\tilde u_0)\frac{\tilde u_1^2}{2} - \eta_1\right)\\
&\quad + \varepsilon^3\left(-\Delta_1 + W'''(\tilde u_0)\tilde u_3 + W^{(4)}(\tilde u_0)\tilde u_1\tilde u_2 + \frac{1}{6}W^{(5)}(\tilde u_0)\tilde u_1^3\right) + O(\varepsilon^4)\Bigg]\\
&\cdot\Bigg[\left(-\Delta_z\tilde u_0 + W'(\tilde u_0)\right) + \varepsilon\left(-\Delta_z\tilde u_1 + \vec\kappa\cdot\nabla_z\tilde u_0 + W''(\tilde u_0)\tilde u_1\right)\\
&\quad + \varepsilon^2\left(-\Delta_z\tilde u_2 + \vec\kappa\cdot\nabla_z\tilde u_1 - \Delta_0\tilde u_0 + W''(\tilde u_0)\tilde u_2 + \frac{1}{2}W'''(\tilde u_0)\tilde u_1^2\right)\\
&\quad + \varepsilon^3\Bigg(-\Delta_z\tilde u_3 + \vec\kappa\cdot\nabla_z\tilde u_2 - \Delta_0\tilde u_1 - \Delta_1\tilde u_0 + W''(\tilde u_0)\tilde u_3\\
&\qquad + W'''(\tilde u_0)\tilde u_1\tilde u_2 + \frac{1}{6}W^{(4)}(\tilde u_0)\tilde u_1^3\Bigg) + O(\varepsilon^4)\Bigg]\\
&\quad + \varepsilon^2(\eta_1-\eta_2)W'(\tilde u_0) + \varepsilon^3(\eta_1-\eta_2)W''(\tilde u_0)\tilde u_1 + O(\varepsilon^4). \qquad (2.30)
\end{aligned}$$

Thus the chemical potential admits an inner expansion of the form (2.28) where

$$\begin{aligned}
\tilde\mu_0 &= \left(-\Delta_z + W''(\tilde u_0)\right)\left(-\Delta_z\tilde u_0 + W'(\tilde u_0)\right), \qquad (2.31)\\
\tilde\mu_1 &= \left(-\Delta_z + W''(\tilde u_0)\right)\left(-\Delta_z\tilde u_1 + \vec\kappa\cdot\nabla_z\tilde u_0 + W''(\tilde u_0)\tilde u_1\right)\\
&\quad + \left(\vec\kappa\cdot\nabla_z + W'''(\tilde u_0)\tilde u_1\right)\left(-\Delta_z\tilde u_0 + W'(\tilde u_0)\right), \qquad (2.32)\\
\tilde\mu_2 &= \left(\Delta_z - W''(\tilde u_0)\right)\left(\Delta_z\tilde u_2 - \vec\kappa\cdot\nabla_z\tilde u_1 + \Delta_0\tilde u_0 - W''(\tilde u_0)\tilde u_2 - \frac{W'''(\tilde u_0)\tilde u_1^2}{2}\right)\\
&\quad + \left(\vec\kappa\cdot\nabla_z + W'''(\tilde u_0)\tilde u_1\right)\left(-\Delta_z\tilde u_1 + \vec\kappa\cdot\nabla_z\tilde u_0 + W''(\tilde u_0)\tilde u_1\right)\\
&\quad + \left(-\Delta_0 + W'''(\tilde u_0)\tilde u_2 + W^{(4)}\frac{\tilde u_1^2}{2} - \eta_1\right)\left(-\Delta_z\tilde u_0 + W'(\tilde u_0)\right)\\
&\quad + (\eta_1-\eta_2)W'(\tilde u_0). \qquad (2.33)
\end{aligned}$$

The quantity $\tilde\mu_3$ is relevant to the asymptotic results we develop; however, we derive its form under the simplification, $\tilde u_1 = 0$, in (2.30).

A key step in the analysis is the matching conditions between the inner and outer solutions. The outer problem is posed on a domain $\Omega\backslash\Gamma$ with a codimension two boundary; accordingly the proper treatment of the matching conditions requires a careful development of the definition of the normal derivatives at the interface Γ. Fixing $x = \phi(s) \in \Gamma$, we take two unit vectors $\mathbf{n}, \mathbf{m} \in \text{span}\{\mathbf{N}^1(x), \mathbf{N}^2(x)\}$ in the normal plane of Γ at x and further specify that $\mathbf{n} = \cos(\theta)\mathbf{N}^1 + \sin(\theta)\mathbf{N}^2$. The usual directional derivative along $\mathbf{n}$ is denoted

$$\partial_{\mathbf{n}} := \mathbf{n}\cdot\nabla_x = \cos\theta\ \mathbf{N}^1\cdot\nabla_x + \sin\theta\ \mathbf{N}^2\cdot\nabla_x, \qquad (2.34)$$

and for $f \in \mathcal{C}^\infty(\Omega\backslash\Gamma)$ we introduce the $\mathbf{n},\mathbf{m}$ limit

$$\partial_{\mathbf{n}}^j f^{\mathbf{m}}(x) := \lim_{h\to 0^+}(\mathbf{n}\cdot\nabla_x)^j f(x + h\mathbf{m}, t) \quad \text{for all } j \geq 0, \qquad (2.35)$$

and the limit of the gradient

$$\nabla_x f^{\mathbf{m}}(x) := \lim_{h\to 0^+} \nabla_x f(x + h\mathbf{m}, t), \tag{2.36}$$

where the limits exist. If $f \in C^1(\Omega)$, then the normal derivative of f will satisfy $\partial_{\mathbf{n}} f^{-\mathbf{m}} = \partial_{\mathbf{n}} f^{\mathbf{m}}$. This motivates the following definition of the jump condition:

$$[\partial_{\mathbf{n}} f^{\mathbf{n}}]_\Gamma(x) := \partial_{\mathbf{n}} f^{\mathbf{n}}(x) - \partial_{\mathbf{n}} f^{-\mathbf{n}}(x), \tag{2.37}$$

which is zero when f has a smooth extension through Γ.

With this notation we examine the matching condition

$$(\mu_0 + \varepsilon\mu_1 + \varepsilon^2\mu_2 + \dots)(x + \varepsilon R\mathbf{n}, t) \approx (\tilde{\mu}_0 + \varepsilon\tilde{\mu}_1 + \varepsilon^2\tilde{\mu}_2 + \dots)(s, R, \theta, t) \tag{2.38}$$

as εR becomes $o(1)$. Expanding the left-hand side about x as $\varepsilon R \to 0^+$, we have

$$\mu_0^{\mathbf{n}} + \varepsilon(\mu_1^{\mathbf{n}} + R\partial_{\mathbf{n}}\mu_0^{\mathbf{n}}) + \varepsilon^2\left(\mu_2^{\mathbf{n}} + R\partial_{\mathbf{n}}\mu_1^{\mathbf{n}} + \frac{1}{2}R^2\partial_{\mathbf{n}}^2\mu_0^{\mathbf{n}}\right) + \dots, \tag{2.39}$$

and equating orders of ε the matching condition (2.38) yields

$$\mu_0^{\mathbf{n}} = \lim_{R\to\infty} \tilde{\mu}_0(s, R, \theta, t), \tag{2.40}$$

$$\mu_1^{\mathbf{n}} + R\partial_{\mathbf{n}}\mu_0^{\mathbf{n}} = \tilde{\mu}_1(s, R, \theta, t) + o(1) \qquad \text{as } R \to \infty, \tag{2.41}$$

$$\mu_2^{\mathbf{n}} + R\partial_{\mathbf{n}}\mu_1^{\mathbf{n}} + \frac{1}{2}R^2\partial_{\mathbf{n}}^2\mu_0^{\mathbf{n}} = \tilde{\mu}_2(s, R, \theta, t) + o(1) \qquad \text{as } R \to \infty, \tag{2.42}$$

$$\mu_3^{\mathbf{n}} + R\partial_{\mathbf{n}}\mu_2^{\mathbf{n}} + \frac{R^2\partial_{\mathbf{n}}^2\mu_1^{\mathbf{n}}}{2} + \frac{R^3\partial_{\mathbf{n}}^3\mu_0^{\mathbf{n}}}{6} = \tilde{\mu}_3(s, R, \theta, t) + o(1) \qquad \text{as } R \to \infty. \tag{2.43}$$

Similarly, we obtain the matching conditions for u,

$$u_0^{\mathbf{n}} = \lim_{R\to\infty} \tilde{u}_0(s, R, \theta, t), \tag{2.44}$$

$$u_1^{\mathbf{n}} + R\partial_{\mathbf{n}}u_0^{\mathbf{n}} = \tilde{u}_1(s, R, \theta, t) + o(1) \qquad \text{as } R \to \infty, \tag{2.45}$$

$$u_2^{\mathbf{n}} + R\partial_{\mathbf{n}}u_1^{\mathbf{n}} + \frac{1}{2}R^2\partial_{\mathbf{n}}^2u_0^{\mathbf{n}} = \tilde{u}_2(s, R, \theta, t) + o(1) \qquad \text{as } R \to \infty. \tag{2.46}$$

3. Fast equilibration to the pore profile. In this section we consider the relaxation of an initial datum and equilibria solution on the fast $T_j = t/\varepsilon^j$ time scales for $j = 2, 1$. Our principle result, presented in Proposition 3.1, is that the flow (3.9), while possessing complex transients, associates to each interface Γ_p a unique, radially symmetric pore profile, U_p, for which the function $U_p(z)$ is at equilibrium on the T_2 and T_1 time scales.

3.1. Time scale $T_2 = t/\varepsilon^2$: Outer expansion. Far from the pore Γ, the solution and chemical potential admit the outer expansion

$$u(x, t) = u_0 + \varepsilon u_1 + \varepsilon^2 u_2 + \varepsilon^3 u_3 + \dots, \tag{3.1}$$

$$\mu(x, t) = \mu_0 + \varepsilon\mu_1 + \varepsilon^2\mu_2 + \dots, \tag{3.2}$$

where

$$u_i = u_i(x, T_2), \quad \mu_i = \mu_i(x, T_2), \quad T_2 = t/\varepsilon^2. \tag{3.3}$$

Substituting the expansion of u into the definition, (1.12), of μ, we determine

$$\mu_0 = W''(u_0)W'(u_0) = G'(u_0), \tag{3.4}$$

$$\mu_1 = \left(W'''(u_0)W'(u_0) + W''(u_0)^2\right) u_1 = G''(u_0)u_1, \tag{3.5}$$

where $G(u) := \frac{1}{2}(W'(u))^2$. Expanding the left- and right-hand sides of (1.12) yields the expressions

$$\partial_{T_2} u_0 = 0, \quad \partial_{T_2} u_1 = 0, \tag{3.6}$$

$$\partial_{T_2} u_2 = \Delta G'(u_0). \tag{3.7}$$

On the T_2 time scale, the solution u is stationary to first and second orders.

3.2. Time scale $T_2 = t/\varepsilon^2$: Inner expansion. We assume an inner expansion for u and μ of the form (2.28). Since $(s, z) = (s(x, T_2), z(x, T_2))$, the time derivative of u takes the form

$$u_t = \varepsilon^{-2}\left(\tilde{u}_{T_2} + \tilde{u}_s \frac{\partial s}{\partial T_2} + \nabla_z \tilde{u} \cdot \frac{\partial z}{\partial T_2}\right).$$

In light of the normal velocity relations (2.20)–(2.21), we obtain

$$\begin{aligned} u_t = -\varepsilon^{-3}\mathbf{V}_{-2} \cdot \nabla_z \tilde{u}_0 + \varepsilon^{-2}\Big(& \tfrac{\partial \tilde{u}_0}{\partial T_2} + \tfrac{\partial \tilde{u}_0}{\partial s}\tfrac{\partial s}{\partial T_2} + \tfrac{\partial \tilde{u}_0}{\partial z_1} z_2 \mathbf{N}^2 \cdot \tfrac{\partial \mathbf{N}^1}{\partial T_2} \\ & + \tfrac{\partial \tilde{u}_0}{\partial z_2} z_1 \mathbf{N}^1 \cdot \tfrac{\partial \mathbf{N}^2}{\partial T_2} - \mathbf{V}_{-2} \cdot \nabla_z \tilde{u}_1 \Big) + O(\varepsilon^{-1}), \end{aligned} \tag{3.8}$$

where $\mathbf{V}_{-2}$ denotes the normal velocity on the T_2 time scale. Matching the ε^{-3} and the ε^{-2} terms in (3.8) with the corresponding terms in the inner Laplacian expansion, (2.29), for the chemical potential μ we find

$$\begin{aligned} \mathbf{V}_{-2} \cdot \nabla_z \tilde{u}_0 &= 0, \\ \tfrac{\partial \tilde{u}_0}{\partial T_2} + \tfrac{\partial \tilde{u}_0}{\partial s}\tfrac{\partial s}{\partial T_2} + \tfrac{\partial \tilde{u}_0}{\partial z_1} z_2 \mathbf{N}^2 \cdot \tfrac{\partial \mathbf{N}^1}{\partial T_2} + \tfrac{\partial \tilde{u}_0}{\partial z_2} z_1 \mathbf{N}^1 \cdot \tfrac{\partial \mathbf{N}^2}{\partial T_2} - \mathbf{V}_{-2} \cdot \nabla_z \tilde{u}_1 &= \Delta_z \tilde{\mu}_0, \end{aligned}$$

where $\tilde{\mu}_0$ is given by (2.31). We are interested in solutions based upon a quasi-stationary radial profile; consequently we assume that the transient dynamics on the T_2 have equilibrated, that is, $\mathbf{V}_{-2} = 0$ and all T_2 partials are zero, so that the system of equations reduces to $\Delta_z \tilde{\mu}_0 = 0$. These assumptions are consistent with equilibria which at leading order have radially symmetric profiles that render $\tilde{\mu}_0 = 0$. Calculations for the T_1 time scale are similar and are omitted. We deduce the following.

PROPOSITION 3.1. *Let U denote the nontrivial, radially symmetric solution of*

$$-\Delta_z U + W'(U) = -\frac{\partial^2 U}{\partial R^2} - \frac{1}{R}\frac{\partial U}{\partial R} - \frac{1}{R^2}\frac{\partial^2 U}{\partial \theta^2} + W'(U) = 0 \tag{3.9}$$

subject to the boundary condition $U \to b_-$ exponentially as $|z| \to \infty$. Then the extension of U off of Γ_ℓ is an equilibrium of (1.12) on the T_2 and T_1 time scales.

Remark 3.2. The existence of a unique, radially symmetric pore profile U_p of (3.9), which consequently also satisfies (1.8), follows from standard results; see [14, section 9.5.2]. In what follows we drop the subscript p from U_p to simplify notation.

A key role is played by the linearization

$$\mathcal{L} := -\Delta_z + W''(U) \tag{3.10}$$

of (3.9) about U. This operator is self-adjoint in the R-weighted inner product and has strictly positive essential spectrum $[W''(b_-), \infty)$ [25]. Moreover, the translational eigenfunctions $\partial_{z_1} U$ and $\partial_{z_2} U$ lie in the kernel of $\mathcal{L}$. For each $m \in \mathbb{N}$ the spaces

$$\mathcal{Z}_m := \{ f(R)\cos(m\theta) + g(R)\sin(m\theta) \,\big|\, f, g \in C^\infty(0,\infty) \}$$

are invariant under the operator $\mathcal{L}$ and mutually orthogonal in $L^2(\Omega)$. Moreover, on these spaces $\mathcal{L}$ reduces to

$$\mathcal{L}\big(f(R)\cos(m\theta) + g(R)(\sin m)\theta\big) = \cos(m\theta)\mathcal{L}_m f + \sin(m\theta)\mathcal{L}_m g,$$

where

$$\mathcal{L}_m := -\frac{\partial^2}{\partial R^2} - \frac{1}{R}\frac{\partial}{\partial R} + \frac{m^2}{R^2} + W''(U). \tag{3.11}$$

Each operator $\mathcal{L}_m$ is self-adjoint on $\mathbb{R}_+$ in the R-weighted inner product, and moreover the operator $\mathcal{L}_1$ is nonnegative with kernel spanned by $\partial_R U$. For $m > 1$ we deduce that each of $\mathcal{L}_m > \mathcal{L}_1$ is strictly positive, while $\mathcal{L}_0 < \mathcal{L}_1$ has a ground state with a negative eigenvalue and possibly a kernel. We address the kernel of $\mathcal{L}_0$ with the following assumption.

ASSUMPTION 3.3. *We assume that the operator $\mathcal{L}_0$ has no kernel, so that*

$$\ker(\mathcal{L}) = \operatorname{span}\{\partial_{z_1} U, \partial_{z_2} U\} = \operatorname{span}\{\partial_R U \cos\theta, \partial_R U \sin\theta\}. \tag{3.12}$$

In particular, the operator $\mathcal{L}_m$ is boundedly invertible for all $m \neq 1$.

We remark that any $f \in L^2(\mathbb{R}^2)$ admits the Fourier expansion

$$f = f_0(R) + \sum_{m=1}^{\infty} \left(f_m(R)\cos(m\theta) + g_m(R)\sin(m\theta) \right),$$

and so long as $\{f_1, g_1\} \perp \ker(\mathcal{L}_1)$, we have the inverse formulation

$$\mathcal{L}^{-1} f = \mathcal{L}_0^{-1} f_0 + \sum_{m=1}^{\infty} \left(\left(\mathcal{L}_m^{-1} f_m(R)\right)\cos(m\theta) + \left(\mathcal{L}_m^{-1} g_m(R)\right)\sin(m\theta) \right).$$

4. The time scale $t = O(1)$. On the t time scale, we perform a regular expansion of the outer solution u and chemical potential μ as in (3.1) and (3.2). The main result, presented in Lemma 4.1, is for a large class of codimension two interfaces Γ_p; the only leading-order equilibrium on the t time scale is the spatially constant solution $u \equiv b_0$.

We proceed by matching the $O(1)$ terms in u_t and $\Delta\mu$, obtaining the nonlinear diffusion equation for u_0,

$$\partial_t u_0 = \Delta\mu_0, \quad \mu_0 = G'(u_0), \tag{4.1}$$

where $G(u) := \frac{1}{2}(W'(u))^2$. Since (4.1) is a gradient flow of the energy $E_G(u) := \int_\Omega G(u)\, dx$, it has stable equilibrium at the minima of G, that is, the zeros of $W'(u)$. In particular, $u_0 = b_-$ is a stable equilibrium.

4.1. Inner expansion. In the inner region, Γ_ℓ, we have an inner expansion, (2.28), of u and μ. As in (3.8) we expand the time derivative of u as

$$u_t = \tilde{u}_t + \tilde{u}_s \frac{\partial s}{\partial t} + \frac{\partial z}{\partial t} \cdot \nabla_z \tilde{u} = -\varepsilon^{-1} \mathbf{V}_0 \cdot \nabla_z \tilde{u}_0 + O(1), \tag{4.2}$$

where $\mathbf{V}_0$ denotes the normal velocity on the t time scale. Matching (4.2) and (2.29), the ε^{-2} and ε^{-1} terms give

$$0 = \Delta_z \tilde{\mu}_0, \tag{4.3}$$

$$-\mathbf{V}_0 \cdot \nabla_z \tilde{u}_0 = \Delta_z \tilde{\mu}_1 - \vec{\kappa} \cdot \nabla_z \tilde{\mu}_0. \tag{4.4}$$

Equation (4.3) is consistent with the leading-order solution $u(x,t) = U(z)$, which renders $\tilde{\mu}_0 = 0$. Consequently, (4.4) simplifies to

$$\mathbf{V}_0 \cdot \nabla_z U = -\Delta_z \tilde{\mu}_1. \tag{4.5}$$

To determine $\mathbf{V}_0$ we must determine an explicit solution for $\tilde{\mu}_1$ in (4.5), subject to matching conditions with the outer solution. Turning to polar coordinates, $z_1 = R\cos\theta, z_2 = R\sin\theta$, we write $\tilde{\mu}_1$ in its Fourier series

$$\tilde{\mu}_1 = A(s,R)\cos\theta + B(s,R)\sin\theta + C(s,R) + \xi(s,R,\theta), \tag{4.6}$$

where

$$\xi(s,R,\theta) = \sum_{m=2}^{\infty} (A_m(s,R)\cos m\theta + B_m(s,R)\sin m\theta). \tag{4.7}$$

The Cartesian Laplacian in z transforms to the familiar polar Laplacian in R and θ, while the left-hand side of (4.5) transforms to

$$\mathbf{V}_0 \cdot \nabla_z U = U'(R)\left(V_{01}\cos\theta + V_{02}\sin\theta\right). \tag{4.8}$$

Substituting these expansions into (4.5) and matching terms yields the system

$$\frac{\partial^2 A}{\partial R^2} + \frac{1}{R}\frac{\partial A}{\partial R} - \frac{1}{R^2}A = -V_{01}U'(R), \tag{4.9}$$

$$\frac{\partial^2 B}{\partial R^2} + \frac{1}{R}\frac{\partial B}{\partial R} - \frac{1}{R^2}B = -V_{02}U'(R), \tag{4.10}$$

$$\frac{\partial^2 C}{\partial R^2} + \frac{1}{R}\frac{\partial C}{\partial R} = 0, \tag{4.11}$$

$$\frac{\partial^2 A_m}{\partial R^2} + \frac{1}{R}\frac{\partial A_m}{\partial R} - \frac{m^2}{R^2}A_m = 0, \qquad m = 2,3,\ldots, \tag{4.12}$$

$$\frac{\partial^2 B_m}{\partial R^2} + \frac{1}{R}\frac{\partial B_m}{\partial R} - \frac{m^2}{R^2}B_m = 0, \qquad m = 2,3,\ldots. \tag{4.13}$$

Excluding singularities, the solutions to (4.12) and (4.13) take the form

$$A_m(s,R) = a_m(s)R^m, \quad B_m(s,R) = b_m(s)R^m, \quad m = 2,3,\ldots, \tag{4.14}$$

while (4.11) yields $C = C_0(s)$, and (4.9) and (4.10) have solutions

$$A(s,R) = C_{01}(s)R - V_{01}(s)a(R), \quad B(s,R) = C_{02}R - V_{02}(s)a(R),$$

where a satisfies

$$a''(R) + \frac{1}{R}a'(R) - \frac{1}{R^2}a(R) = \frac{1}{R^2}\frac{d}{dR}\left(R^3\frac{d}{dR}\left(\frac{a}{R}\right)\right) = U'(R). \tag{4.15}$$

This equation has the inhomogeneous solution

$$a(R) = \frac{1}{R}\int_0^R r\hat{U}\,dr, \tag{4.16}$$

where we have introduced the shifted pore profile $\hat{U} := U_p - b_-$ which is positive and tends to zero exponentially as $R \to \infty$. The chemical potential $\tilde{\mu}_1$ takes the general form

$$\begin{aligned}\tilde{\mu}_1 = {} & C_0(s) + (C_{01}(s)R - V_{01}(s)a(R))\cos\theta + (C_{02}R - V_{02}a(R))\sin\theta \\ & + \sum_{m=2}^{\infty}\Big(a_m(s)R^m\cos m\theta + b_m(s)R^m\sin m\theta\Big).\end{aligned} \tag{4.17}$$

However, simplifying the relation (2.32) between $\tilde{\mu}_1$ and $\tilde{u}_1$, we find that

$$\tilde{\mu}_1 = \mathcal{L}^2\tilde{u}_1, \tag{4.18}$$

where we have introduced the linearization about U,

$$\mathcal{L} := -\Delta_z + W''(U). \tag{4.19}$$

In particular, $\tilde{\mu}_1$ is in the range of $\mathcal{L}$ and hence perpendicular to $\ker(\mathcal{L})$. From Assumption 3.3 this requires

$$\int_{\mathbb{R}^2}\tilde{\mu}_1\partial_{z_i}\hat{U}\,dz = 0 \tag{4.20}$$

for $i = 1, 2$. From orthogonality in θ, the only nontrivial condition is imposed on the $\sin\theta$ and $\cos\theta$ terms in $\tilde{\mu}_1$. For $i = 1, 2$, the condition (4.20) reduces to

$$0 = \int_0^{\infty}(C_{0i}R - V_{0i}a(R))\,U'(R)R\,dR, \tag{4.21}$$

which after integration by parts yields the relation

$$C_{0i}(s) = \frac{S_2}{2S_1}V_{0i}(s), \tag{4.22}$$

where we have introduced

$$S_1 := \int_0^{\infty}\hat{U}(R)R\,dR > 0 \quad \text{and} \quad S_2 := \int_0^{\infty}\hat{U}^2(R)R\,dR > 0, \tag{4.23}$$

defined in terms of the shifted pore profile, $\hat{U} = U_p - b_-$.

The normal velocity $\mathbf{V}$ is determined through matching conditions between the inner and the outer expansions. From (2.41) we see that $\tilde{\mu}_1$ grows at most linearly as $R \to \infty$ and

$$\lim_{R\to\infty}\frac{\partial\tilde{\mu}_1}{\partial R}(s, R, \theta, t) = \partial_{\mathbf{n}}\mu_0^{\mathbf{n}} = \cos\theta\,\mathbf{N}^1\cdot\nabla_x\mu_0^{\mathbf{n}} + \sin\theta\,\mathbf{N}^2\cdot\nabla_x\mu_0^{\mathbf{n}}. \tag{4.24}$$

Comparing these conditions with (4.17), we deduce that $a_m = b_m = 0$, $m \geq 2$. Moreover, since

$$\frac{\partial \tilde{\mu}_1}{\partial R}(s, R, \pi + \theta, t) = -\frac{\partial \tilde{\mu}_1}{\partial R}(s, R, \theta, t), \tag{4.25}$$

we deduce from (4.24) that the $\partial_{\mathbf{n}} \mu_0^{\mathbf{n}}$ satisfies the jump condition (see (2.37))

$$[\partial_{\mathbf{n}} \mu_0^{\mathbf{n}}]_\Gamma = 0 \tag{4.26}$$

for any choice of normal vector $\mathbf{n}$. We simplify the left-hand side of (4.24):

$$\frac{\partial \tilde{\mu}_1}{\partial R}(s, R, \theta, t) = V_{01}\left(\frac{S_2}{2S_1} - \frac{\partial a}{\partial R}\right)\cos\theta + V_{02}\left(\frac{S_2}{2S_1} - \frac{\partial a}{\partial R}\right)\sin\theta. \tag{4.27}$$

Equating coefficients of $\sin\theta$ and $\cos\theta$ in (4.24) yields

$$\mathbf{N}^i \cdot \nabla_x \mu_0^{\mathbf{N}^i} = V_{0i}\left(\frac{S_2}{2S_1} - \lim_{R\to\infty}\frac{\partial a}{\partial R}\right), \tag{4.28}$$

and since a decays as $R \to \infty$ we find that

$$V_{0i} = \frac{2S_1}{S_2}\mathbf{N}^i \cdot \nabla_x \mu_0^{\mathbf{N}^i} \tag{4.29}$$

for $i = 1, 2$. Combining (4.1), (4.26), and (4.29) yields the sharp interface limit problem for the evolution of Γ,

$$\partial_t u_0 = \Delta \mu_0 \qquad \text{in } \Omega \setminus \Gamma(t), \tag{4.30}$$

$$\mathbf{n} \cdot \nabla_x u_0 = 0 \qquad \text{on } \partial\Omega, \tag{4.31}$$

$$u_0 = b_- \qquad \text{on } \Gamma, \tag{4.32}$$

$$[\partial_{\mathbf{n}} \mu_0^{\mathbf{n}}]_\Gamma = 0 \qquad \text{on } \Gamma, \text{ for all normal vectors } \mathbf{n} \text{ of } \Gamma, \tag{4.33}$$

$$V_{0i} = \frac{2S_1}{S_2}\mathbf{N}^i \cdot \nabla_x \mu_0^{\mathbf{N}^i} \qquad \text{for all } x \in \Gamma(t),\ i = 1, 2, \tag{4.34}$$

where the chemical potential $\mu_0 = W''(u_0)W'(u_0)$. The analysis of the transient solutions of (4.30)–(4.34) is beyond the scope of this paper; however, the equilibria are trivial.

LEMMA 4.1. *Assume that the codimension two interface $\Gamma \subset (\Omega)$ has finite one-dimensional Hausdorff measure. Then the only equilibrium solution of* (4.30)–(4.34) *is the trivial solution $u_0(x, t) \equiv b_-$; however, the curve Γ can have arbitrary shape.*

Proof. At equilibrium we have $\Delta\mu_0 = 0$ in $\Omega\backslash\Gamma$ subject to $\mathbf{n} \cdot \nabla_x \mu_0 = 0$ and $\mu_0 = 0$ on Γ. From classic regularity theory it follows that $\mu_0 \in \mathcal{C}^2(\Omega\backslash\Gamma)$ and is bounded over all of Ω. Since the one-dimensional Hausdorff measure of Γ is finite, it has zero one-dimensional capacity, and hence μ_0 is harmonic on all of Ω; see [30] or the example on page 29 of [15]. By the strong maximum principle it follows that μ_0, and hence u_0, are constant. Since $u_0 = b_-$ on Γ, we deduce that $u_0 \equiv b_-$. ∎

We subsequently assume the system has achieved equilibrium on the t time scale.

5. The time scale $t_1 = \varepsilon t$: Quenched mean-curvature flow. On the slow time scale, $t_1 = \varepsilon t$, we use a matched inner-outer asymptotic expansion to derive a curvature driven flow for the normal velocity of the closed-loop pore structures. However, the normal velocity is quenched by the leading-order outer chemical potential, $\mu_1 = \mu_1(t_1)$, which is driven to zero at an exponential rate.

5.1. Outer expansion. On the outer scale, matching the terms in u_t and $\Delta\mu$ in (1.12), we obtain

$$0 = \Delta\mu_0, \quad \mu_0 = W''(u_0)W'(u_0), \tag{5.1}$$

$$\partial_{t_1} u_0 = \Delta\mu_1. \tag{5.2}$$

By assumption the system (4.30)–(4.32) has reached the equilibrium $u_0 = b_-$ in $\Omega \setminus \Gamma(t)$. In this case $\mu_0 = W''(b_-)W'(b_-) = 0$ and

$$\mu_1 = \big(W'''(u_0)W'(u_0) + W''(u_0)^2\big)u_1 = \alpha_-^2 u_1, \tag{5.3}$$

so that (5.2) reduces to

$$\Delta u_1 = 0 \tag{5.4}$$

in $\Omega \setminus \Gamma(t)$.

5.2. Inner expansion. Forming an inner expansion, (2.28), for u and μ, the time derivative of u admits the expansion

$$u_t = \varepsilon\left(\tilde{u}_{t_1} + \frac{\partial\tilde{u}}{\partial s}\frac{\partial s}{\partial t_1}\right) + \varepsilon\frac{\partial z}{\partial t_1}\cdot\nabla_z\tilde{u} = -\mathbf{V}_1\cdot\nabla_z\tilde{u}_0 + O(\varepsilon), \tag{5.5}$$

where we have introduced the normal velocity $\mathbf{V}_1 = (V_{11}, V_{12})^t$ on the t_1 time scale. Matching the ε^{-2}, ε^{-1}, and ε^0 terms in (5.5) and (2.29) yields

$$0 = \Delta_z\tilde{\mu}_0, \tag{5.6}$$

$$0 = \Delta_z\tilde{\mu}_1 - \vec{\kappa}\cdot\nabla_z\tilde{\mu}_0, \tag{5.7}$$

$$-\mathbf{V}_1\cdot\nabla_z\tilde{u}_0 = \Delta_z\tilde{\mu}_2 - \vec{\kappa}\cdot\nabla_z\tilde{\mu}_1 + \Delta_0\tilde{\mu}_0. \tag{5.8}$$

The matching condition (2.40) and (5.6) imply that $\tilde{\mu}_0 = 0$, and hence $\tilde{u}_0 = U$ and (5.7) simplifies to

$$\Delta_z\tilde{\mu}_1 = 0. \tag{5.9}$$

This equation has solutions of the form

$$\tilde{\mu}_1 = C(s) + \sum_{m=1}^{\infty}\Big(a_m(s)R^m\cos m\theta + b_m(s)R^m\sin m\theta\Big). \tag{5.10}$$

Since $\mu_0 = 0$, the matching condition (2.41) implies that $a_m = b_m = 0$ for all $m \geq 1$, and hence $\tilde{\mu}_1 = \tilde{\mu}_1(s,t)$ is independent of z. Since $\tilde{u}_0 = U$, (2.32) reduces to

$$\tilde{\mu}_1 = \mathcal{L}(\mathcal{L}\tilde{u}_1 + \vec{\kappa}\cdot\nabla_z U) = \mathcal{L}^2\tilde{u}_1. \tag{5.11}$$

To invert $\mathcal{L}^2$ we introduce the following functions.

LEMMA 5.1. *For $j = 1, 2$ there exist radially symmetric functions Φ_j which converge exponentially to asymptotic values α_-^{-j} as $R \to \infty$ such that $\Phi_j - \alpha_-^{-j} \in \ker(\mathcal{L})^\perp$ and which solve*

$$\mathcal{L}\Phi_1 = 1 \quad \text{and} \quad \mathcal{L}\Phi_2 = \Phi_1. \tag{5.12}$$

Proof. Since U converges to b_- at an exponential rate as $R \to \infty$, (5.12) is equivalent to

$$\mathcal{L}(\Phi_1 - \alpha_-^{-1}) = 1 - W''(U)/W''(b_-),$$

where the right-hand side lies in $\ker(\mathcal{L})^\perp \subset L^2$. Since the essential spectrum of $\mathcal{L}$ is bounded away from the origin, the operator is Fredholm of index zero, and this problem has a unique solution which lies in $\ker(L)^\perp$. Since the right-hand side is radial, the solution is, too. A similar argument holds for Φ_2. ∎

Using Lemma 5.1, we solve (5.11) for $\tilde{u}_1$,

$$\tilde{u}_1 = \tilde{\mu}_1 \Phi_2(R), \tag{5.13}$$

and (5.8) simplifies to

$$\Delta_z \tilde{\mu}_2 = -\mathbf{V}_1 \cdot \nabla_z U. \tag{5.14}$$

As in section 4, this equation has a solution of the form

$$\tilde{\mu}_2 = C_4(s) + (C_{11}(s)R - V_{11}a(R))\cos\theta + (C_{12}(s)R - V_{12}a(R))\sin\theta + \xi_2, \tag{5.15}$$

where a is as defined in (4.16) and ξ_2 takes the form of the final term in (4.17). On the other hand, since $\tilde{u}_0 = U$ and $\tilde{u}_1$ satisfies (5.13), (2.33) simplifies to

$$\begin{aligned}\tilde{\mu}_2 = \mathcal{L}\left(\mathcal{L}\tilde{u}_2 + \vec{\kappa}\cdot\nabla_z\tilde{u}_1 - \Delta_0 U + \frac{1}{2}W'''(U)\tilde{u}_1^2\right)\\ + \left(\vec{\kappa}\cdot\nabla_z + W'''(U)\tilde{u}_1\right)\left(\mathcal{L}\tilde{u}_1 + \vec{\kappa}\cdot\nabla_z U\right) + (\eta_1 - \eta_2)W'(U),\end{aligned} \tag{5.16}$$

which can be rewritten as

$$\mathcal{L}\left(\mathcal{L}\tilde{u}_2 + \tilde{\mu}_1\vec{\kappa}\cdot\nabla_z\Phi_2 + (z\cdot\vec{\kappa})\vec{\kappa}\cdot\nabla_z U + \frac{1}{2}W'''(U)\tilde{\mu}_1^2\Phi_2^2\right) = \mathcal{R}_2, \tag{5.17}$$

where we have introduced

$$\begin{aligned}\mathcal{R}_2 := \tilde{\mu}_2 - (\vec{\kappa}\cdot\nabla_z)^2 U - \tilde{\mu}_1(\vec{\kappa}\cdot\nabla_z\Phi_1 + W'''(U)\Phi_2\vec{\kappa}\cdot\nabla_z U) - \tilde{\mu}_1^2 W'''(U)\Phi_1\Phi_2\\ - (\eta_1 - \eta_2)W'(U).\end{aligned}$$

In particular, we may solve for $\tilde{u}_2$ if and only if $\mathcal{R}_2 \in \ker(\mathcal{L})^\perp$. Addressing these two conditions term by term, we calculate that

$$\begin{aligned}\int_{\mathbb{R}^2} \tilde{\mu}_2 \frac{\partial U}{\partial z_i}\, dz &= \pi\left(C_{1i}\int_0^\infty U'(r)r^2\, dr - V_{1i}\int_0^\infty a(r)U'(r)r\, dr\right)\\ &= -\pi\left(2C_{1i}S_1 - V_{1i}S_2\right),\end{aligned} \tag{5.18}$$

where S_1 and S_2 are as introduced in (4.23). The terms $(\kappa\cdot\nabla_z)^2 U \in (\mathcal{Z}_0 + \mathcal{Z}_2)$ and $W'''(U)\Phi_1\Phi_2 \in \mathcal{Z}_0$ are orthogonal to $\partial_{z_i}U \in \mathcal{Z}_1$, while

$$(\mathcal{R}_2 - \tilde{\mu}_2, \partial_{z_i}U) = -\pi\tilde{\mu}_1\kappa_i\int_0^\infty U'\big(\Phi_1' + W'''(U)\Phi_2 U'\big)R\, dR. \tag{5.19}$$

LEMMA 5.2. *The operator* $\mathcal{L}$ *satisfies*

$$\mathcal{L}\left(\frac{1}{2}RU'\right) = \frac{1}{2}\mathcal{L}_0(RU') = -\Delta_z U = -\left(U'' + \frac{1}{R}U'\right), \tag{5.20}$$

$$\mathcal{L}(\Delta_z U) = \mathcal{L}_0\left(U'' + \frac{1}{R}U'\right) = -W'''(U)|\nabla U|^2 = -W'''(U)U'^2. \tag{5.21}$$

Integrating by parts on the Φ_1' term in (5.19) and using (5.20)–(5.21), we obtain

$$\begin{aligned}(\mathcal{R}_2 - \tilde{\mu}_2, \partial_{z_i} U) &= -\frac{\pi}{2}\tilde{\mu}_1\kappa_i \int_0^\infty \left(\Phi_1 \mathcal{L}(RU') + \Phi_2 \mathcal{L}^2(RU')\right) R\, dR \\ &= -\pi\tilde{\mu}_1\kappa_i \int_0^\infty R^2 U' dR = 2\pi\tilde{\mu}_1\kappa_i S_1. \end{aligned} \tag{5.22}$$

Combining (5.18) and (5.22) the solvability condition reduces to

$$\mathbf{C}_1(s) = \tilde{\mu}_1 \vec{\kappa} + \frac{S_2}{2S_1}\mathbf{V}_1. \tag{5.23}$$

The normal velocity $\mathbf{V}_1$ is determined through the matching condition (2.42). Since $\mu_0 = 0$, this condition reduces to

$$\lim_{R\to\infty} \frac{\partial \tilde{\mu}_2}{\partial R}(s, R, \theta) = \partial_{\mathbf{n}} \mu_1^{\mathbf{n}}(s, \theta) = \mathbf{n} \cdot \nabla_x \mu_1^{\mathbf{n}}, \tag{5.24}$$

where $\mathbf{n} := \cos\theta\, \mathbf{N}^1 + \sin\theta\, \mathbf{N}^2$. As a consequence, $\xi_2 = 0$ in (5.15) and

$$\lim_{R\to\infty} \left((C_{11}(s) - V_{11}a'(R))\cos\theta + (C_{12}(s) - V_{12}a'(R))\sin\theta\right) = \mathbf{n} \cdot \nabla_x \mu_1^{\mathbf{n}}. \tag{5.25}$$

We deduce that $[\partial_{\mathbf{n}} \mu_1^{\mathbf{n}}]_\Gamma = 0$, and, moreover, $a'(R) \to 0$ as $R \to \infty$. Using (5.23) and equating coefficients of $\sin\theta$ and $\cos\theta$, we obtain

$$V_{1i} = \frac{2S_1}{S_2}\left(\mathbf{N}^i \cdot \nabla_x \mu_1^{\mathbf{N}^i} - \tilde{\mu}_1(s)\kappa_i\right). \tag{5.26}$$

5.3. Sharp-interface limit. On the t_1 time scale, the evolution of the interface, Γ, is given by the normal velocity

$$V_i = \frac{2S_1}{S_2}\left(\mathbf{N}^i \cdot \nabla_x \mu_1^{\mathbf{N}^i} - \mu_1\kappa_i\right) \quad \text{on } \Gamma,\ i = 1, 2, \tag{5.27}$$

where μ_1 is the solution of the elliptic system

$$\Delta\mu_1 = 0 \qquad \text{in } \Omega \setminus \Gamma, \tag{5.28}$$

$$\mathbf{n} \cdot \nabla_x \mu_1 = 0 \qquad \text{on } \partial\Omega, \tag{5.29}$$

$$[\partial_{\mathbf{n}} \mu_1^{\mathbf{n}}]_\Gamma = 0 \qquad \text{on } \Gamma, \text{ for all normal vectors } \mathbf{n} \text{ of } \Gamma. \tag{5.30}$$

The inner chemical potential satisfies $\mu_1 = \tilde{\mu}_1(s, t_1)$ on Γ. However, the following lemma shows that the solutions, μ_1 to this system are trivial.

LEMMA 5.3. *Suppose* $\mu_1 \in C^2(\Omega \setminus \Gamma) \cap C(\bar{\Omega})$ *satisfies* (5.28) *and* (5.29) *and* Γ *has finite one-dimensional Hausdorff measure; then* μ_1 *is a spatial constant.*

Proof. By the arguments of Lemma 4.1 we deduce that $\Delta\mu_1 = 0$ on all of Ω. The result then follows from the strong maximum principle. ∎

It remains to determine the spatially constant value $\mu_1 = \mu_1(t_1)$, which is determined by mass conservation. Since $\nabla_x \mu_1 = 0$ the normal velocity reduces to

$$\mathbf{V} = -\frac{2S_1}{S_2}\mu_1 \vec{\kappa}. \tag{5.31}$$

Denoting the total mass of the minority phase by M_0, we decompose it as

$$M_0 = \int_{\Omega\setminus\Gamma_\ell} (u - b_-)\, dx + \int_{\Gamma_\ell} (u - b_-) dx. \tag{5.32}$$

Solving (5.3) for μ_1 the outer integral becomes

$$\begin{aligned} \int_{\Omega\setminus\Gamma_\ell} (u - b_-)\, dx &= \int_{\Omega\setminus\Gamma_\ell} \varepsilon\alpha_-^{-2}\mu_1\, dx + O(\varepsilon^2) \\ &= \varepsilon\alpha_-^{-2}\mu_1(|\Omega| - |\Gamma_\ell|) + O(\varepsilon^2), \end{aligned} \tag{5.33}$$

while absorbing the $|\Gamma_\ell|$ term in (5.33) into the inner integral, changing variables, and recalling (2.22) yields

$$\begin{aligned} \int_{\Gamma_\ell} (\tilde{u} - b_-) - \varepsilon\alpha_-^{-2}\mu_1\, dx &= \int_\Gamma \int_{\mathbb{R}^2} \left((\tilde{u} - b_-) - \varepsilon\alpha_-^{-2}\mu_1\right) J(s,z)\, ds\, dz \\ &= \int_\Gamma \int_{\mathbb{R}^2} \left(\hat{U} + \varepsilon(\tilde{u}_1 - \mu_1\alpha_-^{-2})\right) (\varepsilon^2 - \varepsilon^3 z\cdot\vec{\kappa})\, dz\, ds \\ &= 2\pi|\Gamma| \left(S_1\varepsilon^2 + \mu_1 S_3\varepsilon^3\right) + O(\varepsilon^4|\Gamma|), \end{aligned} \tag{5.34}$$

where the shifted pore profile $\hat{U}$ is orthogonal to z and we introduced

$$S_3 := \int_0^\infty (\Phi_2 - \alpha_-^{-2})\, R\, dR > 0. \tag{5.35}$$

Combining (5.34) and (5.33), we have

$$M_0 = \alpha_-^{-2}\mu_1|\Omega|\varepsilon + 2\pi S_1|\Gamma|\varepsilon^2 + 2\pi\mu_1|\Gamma|S_3\varepsilon^3 + O(\varepsilon^4|\Gamma|). \tag{5.36}$$

We consider this balance under various configurations.

5.3.1. $|\Gamma|$ is $O(\varepsilon^{-1})$. This scaling is consistent with Principle Result 1.1. We expand the length of Γ as

$$|\Gamma| = \varepsilon^{-1}\gamma_{-1} + \gamma_0 + \varepsilon\gamma_1 + O(\varepsilon^2), \tag{5.37}$$

and, writing $M_0 = \varepsilon\tilde{M}_0 + \varepsilon^2\tilde{M}_1 + O(\varepsilon^2)$, (5.36) yields

$$\tilde{M}_0 = \alpha_-^{-2}|\Omega|\mu_1 + 2\pi S_1\gamma_{-1}. \tag{5.38}$$

Taking the t_1 derivative of this expression, we determine that

$$\frac{d|\Gamma|}{dt_1} = \varepsilon^{-1}\frac{d\gamma_{-1}}{dt_1} + O(1) = -\varepsilon^{-1}\frac{|\Omega|}{2\pi\alpha_-^2 S_1}\frac{d\mu_1}{dt_1} + O(1). \tag{5.39}$$

On the other hand,

$$\frac{d|\Gamma|}{dt_1} = -\int_\Gamma \mathbf{V}\cdot\vec{\kappa}\, ds = \frac{2S_1}{S_2}\mu_1 \int_\Gamma |\vec{\kappa}|^2\, ds. \tag{5.40}$$

Equating the two expressions yields the leading-order evolution equation

$$\frac{d\mu_1}{dt_1} = -\varepsilon \frac{4\pi\alpha_-^2 S_1^2}{|\Omega| S_2} \mu_1 \int_\Gamma |\vec{\kappa}|^2 \, ds. \tag{5.41}$$

From (4.23), $S_1, S_2 > 0$, and μ_1 decays exponentially to 0 on the t_1 time scale, so long as $|\Gamma| = |\Gamma_p|$ scales as ε^{-1} and has $O(1)$ curvature. This result is consistent with our assumption of quasi equilibrium (see Definition 1.1). The transient behavior of the coupled system (5.31)–(5.41) merits further study. The normal velocity is driven by either a quenched mean-curvature flow for $\mu_1 < 0$ or a quenched backward mean-curvature flow for $\mu_1 > 0$. For the quenched mean-curvature flow it is relatively straightforward to determine criteria on initial data for which μ_1 quenches to zero before the curvature terms can form singularities. A more intriguing case is the possible well-posedness of the quenched backward curvature flow for interfaces whose parameterization is analytic.

5.3.2. $|\Gamma|$ is $O(1)$. Since the total mass M_0 of the minority species is conserved, we see that $\mu_1'(t_1) = O(\varepsilon)$, and μ_1 is constant on this time scale. If, moreover, $M_0 = O(\varepsilon^2)$, then $\mu_1 = 0$ to leading order.

6. Length-preserving Willmore flow on the slow time scale. In this section we derive the geometric flow for codimension two pore profiles on the $t_2 = \varepsilon^2 t$ time scale, coupled to the far-field chemical potential. We assume quasi equilbrium; that is, all processes have relaxed to equilibrium on the t_1 time scale, and $\mu_0 = \mu_1 \equiv 0$. We find that well-separated collections of closed-loop pores evolve according to a length-preserving Willmoresque flow (6.34) coupled to the mass conservation relation (6.44).

6.1. Outer expansion. On the slow time scale, $t_2 = \varepsilon^2 t$, from the result of section 5, the outer expansion takes the form

$$u = u_0 + \varepsilon^2 u_2 + \varepsilon^3 u_3 + \dots, \tag{6.1}$$

$$\mu = \varepsilon^2 \mu_2 + \varepsilon^3 \mu_3 + \dots. \tag{6.2}$$

Since $u_0 = b_-$, we see that $\partial_t u = O(\varepsilon^4)$, and matching the terms in (1.12), we find

$$\Delta \mu_2 = 0. \tag{6.3}$$

6.2. Inner expansion. Similarly, the inner expansion reduces to

$$u(x,t) = \tilde{u}(s,z,t) = \tilde{u}_0 + \varepsilon^2 \tilde{u}_2 + \varepsilon^3 \tilde{u}_3 + \dots, \tag{6.4}$$

$$\mu(x,t) = \tilde{\mu}(s,z,t) = \varepsilon^2 \tilde{\mu}_2 + \varepsilon^3 \tilde{\mu}_3 + \dots, \tag{6.5}$$

where $\tilde{u}_0 = U$ and the time derivative takes the form

$$u_t = \varepsilon^2 \left(\tilde{u}_{t_2} + \frac{\partial \tilde{u}}{\partial s} \frac{\partial s}{\partial t_2} \right) + \varepsilon^2 \frac{\partial z}{\partial t_2} \cdot \nabla_z \tilde{u} = -\varepsilon \mathbf{V}_2 \cdot \nabla_z \tilde{u}_0 + O(\varepsilon^2), \tag{6.6}$$

where $\mathbf{V}_2 = (V_{21}, V_{22})^t$ is the normal velocity on the t_2 time scale. Matching terms in (6.6) and (2.29), we arrive at

$$0 = \Delta_z \tilde{\mu}_2, \tag{6.7}$$

$$-\mathbf{V}_2 \cdot \nabla_z U = \Delta_z \tilde{\mu}_3 - \vec{\kappa} \cdot \nabla_z \tilde{\mu}_2. \tag{6.8}$$

As at the previous time scales, matching conditions imply that $\tilde{\mu}_2 = \tilde{\mu}_2(s)$ is constant in R and θ, depending only upon the position along the curve Γ. Moreover, the relation (2.33) reduces to

$$\tilde{\mu}_2 = \mathcal{L}^2 \tilde{u}_2 - (\vec{\kappa} \cdot \nabla_z)^2 U + (\eta_1 - \eta_2)\Delta_z U. \tag{6.9}$$

We solve this equation via the following lemma.

LEMMA 6.1. *For $i, j = 1, 2$, there exist unique $\Phi_{ij} \in (\mathcal{Z}_0 + \mathcal{Z}_2) \perp \ker(\mathcal{L})$ such that*

$$\mathcal{L}^2 \Phi_{ij} = \frac{\partial^2 U}{\partial z_i \partial z_j}. \tag{6.10}$$

Moreover, these functions take the form

$$\begin{aligned} \Phi_{11} &= \Phi_3(R) + \Phi_4(R)\cos 2\theta, \\ \Phi_{12} &= \Phi_{21} = \Phi_4(R)\sin 2\theta, \\ \Phi_{22} &= \Phi_3(R) - \Phi_4(R)\cos 2\theta, \end{aligned} \tag{6.11}$$

where Φ_3 and Φ_4 depend only upon R.

Proof. The existence follows from Assumption 3.3 since $\frac{\partial^2 U}{\partial z_i z_j} \perp \ker(\mathcal{L})$ for $i, j = 1, 2$. To derive the functional form (6.11) we calculate that

$$\begin{aligned} U_{z_1 z_1} &= \frac{1}{2}\left(U'' + \frac{1}{R}U'\right) + \frac{1}{2}\left(U'' - \frac{1}{R}U'\right)\cos 2\theta \\ &= -\frac{1}{4}\left(\mathcal{L}_0 + \cos 2\theta\, \mathcal{L}_2\right)(RU'), \end{aligned} \tag{6.12}$$

$$U_{z_1 z_2} = \frac{1}{2}\left(U'' - \frac{1}{R}U'\right)\sin 2\theta = -\frac{1}{4}\sin 2\theta\, \mathcal{L}_2(RU'), \tag{6.13}$$

$$\begin{aligned} U_{z_2 z_2} &= \frac{1}{2}\left(U'' + \frac{1}{R}U'\right) - \frac{1}{2}\left(U'' - \frac{1}{R}U'\right)\cos 2\theta \\ &= -\frac{1}{4}\left(\mathcal{L}_0 - \cos 2\theta\, \mathcal{L}_2\right)(RU'). \end{aligned} \tag{6.14}$$

By Assumption 3.3 the operators $\mathcal{L}_m$ are boundedly invertible for $m \neq 1$. From (5.20) it follows that (6.11) holds with

$$\Phi_3 := \frac{1}{2}\mathcal{L}_0^{-2}\left(U'' + \frac{1}{R}U'\right) = -\frac{1}{4}\mathcal{L}_0^{-1}(RU'), \tag{6.15}$$

$$\Phi_4 := \frac{1}{2}\mathcal{L}_2^{-2}\left(U'' - \frac{1}{R}U'\right) = -\frac{1}{4}\mathcal{L}_2^{-1}(RU'). \qquad \square \tag{6.16}$$

Using Lemmas 5.1 and 6.1, we solve (6.9) for $\tilde{u}_2$ in the form

$$\begin{aligned} \tilde{u}_2 &= \tilde{\mu}_2\Phi_2 + \sum_{i,j}\kappa_i\kappa_j\Phi_{ij} - (\eta_1 - \eta_2)(\Phi_{11} + \Phi_{22}) \\ &= \tilde{\mu}_2\Phi_2 + \left(|\vec{\kappa}|^2 - 2(\eta_1 - \eta_2)\right)\Phi_3 + \left((\kappa_1^2 - \kappa_2^2)\cos 2\theta + 2\kappa_1\kappa_2 \sin 2\theta\right)\Phi_4. \end{aligned} \tag{6.17}$$

Since $\tilde{\mu}_2$ is independent of z, (6.8) simplifies to

$$\Delta_z \tilde{\mu}_3 = -\mathbf{V}_2 \cdot \nabla_z U. \tag{6.18}$$

As in sections 4 and 5, the matching conditions yield a solution of the form

$$\tilde{\mu}_3 = C_3(s) + (C_{21}(s)R - V_{21}a(R))\cos\theta + (C_{22}(s)R - V_{22}a(R))\sin\theta, \tag{6.19}$$

where the functions C_3 and $\mathbf{C}_2 := (C_{21}, C_{22})^t$ are to be determined. Returning to (2.30), using $\tilde{u}_0 = U$ and $\tilde{u}_1 = 0$, and recalling the definition (2.26) of Δ_0, we derive the expression

$$\mathcal{R}_3 = \mathcal{L}\Big(\mathcal{L}\tilde{u}_3 + \vec{\kappa}\cdot\nabla_z\tilde{u}_2 - \Delta_1\tilde{u}_0\Big), \tag{6.20}$$

where we have introduced

$$\begin{aligned}\mathcal{R}_3 := \tilde{\mu}_3 &- \vec{\kappa}\cdot\nabla_z\Big(\mathcal{L}\tilde{u}_2 + (z\cdot\vec{\kappa})\vec{\kappa}\cdot\nabla_z U\Big)\\ &- \Big((z\cdot\vec{\kappa})\vec{\kappa}\cdot\nabla_z + W'''(U)\tilde{u}_2 - (\partial_s^2 + \eta_1)\Big)(\vec{\kappa}\cdot\nabla_z U).\end{aligned} \tag{6.21}$$

We may solve for $\tilde{u}_3$ if and only if $\mathcal{R}_3 \in \ker(\mathcal{L})^\perp$. We address each term in this solvability condition in turn. As in (5.18), we have

$$\int_{\mathbb{R}^2} \tilde{\mu}_3 U_{z_i}\, dz = -\pi(2C_{2i}S_1 - V_{2i}S_2). \tag{6.22}$$

Using (6.12)–(6.14) and (6.17) on the $\mathcal{L}\tilde{u}_2$ term yields

$$\begin{aligned}(\vec{\kappa}\cdot\nabla_z(\mathcal{L}\tilde{u}_2), U_{z_1})_{L^2} &= -\left(\mathcal{L}\tilde{u}_2, \kappa_1 U_{z_1z_1} + \kappa_2 U_{z_1z_2}\right)_{L^2}\\ &= \frac{1}{4}\left(\mathcal{L}\tilde{u}_2, \kappa_1\mathcal{L}_0(RU') + (\kappa_1\cos 2\theta + \kappa_2\sin 2\theta)\mathcal{L}_2(RU')\right)_{L^2}\\ &= \frac{1}{4}\left(\tilde{\mu}_2 + \left(\frac{1}{2}|\vec{\kappa}|^2 - \eta_1 + \eta_2\right)\frac{1}{R}(RU')', \kappa_1 RU'\right)_{L^2}\\ &\quad + \frac{1}{8}\left((\kappa_1^2 - \kappa_2^2)\kappa_1\cos^2 2\theta + 2\kappa_1^2\kappa_2\sin^2 2\theta\right)\left(U'' - \frac{1}{R}U', RU'\right)_{L^2}.\end{aligned}$$

Switching to polar coordinates and carrying out the θ integration, we obtain

$$\begin{aligned}(\vec{\kappa}\cdot\nabla_z(\mathcal{L}\tilde{u}_2), U_{z_i})_{L^2} &= \frac{\pi}{2}\int_0^\infty \kappa_i\tilde{\mu}_2 R^2U' + \left(\frac{1}{2}|\vec{\kappa}|^2 - \eta_1 + \eta_2\right)\kappa_i(RU')'RU'\,dR\\ &\quad + \frac{\pi}{8}|\vec{\kappa}|^2\kappa_i\int_0^\infty (U'' - \frac{1}{R}U')R^2U'\,dR\\ &= -\pi\left(\tilde{\mu}_2 S_1 + \frac{|\vec{\kappa}|^2}{4}S_4\right)\kappa_i\end{aligned} \tag{6.23}$$

for $i = 1, 2$, where we have introduced

$$S_4 := \int_0^\infty (U')^2 R\,dR > 0. \tag{6.24}$$

For the other $\tilde{u}_2$ term, using (5.20) and (5.21), we find

$$(W'''(U)\tilde{u}_2\vec{\kappa}\cdot\nabla_z U, U_{z_1})_{L^2} = \frac{1}{2}\int_{\mathbb{R}^2}\tilde{u}_2(\kappa_1\cos^2\theta + \kappa_2\cos\theta\sin\theta)\mathcal{L}_0^2(RU')\,dz.$$

Substituting (6.17) for $\tilde{u}_2$, the θ-integrals are zero, except for the product of the $\cos^2\theta$ term and the θ-independent terms of $\tilde{u}_2$. For $i = 1, 2$ these terms yield

$$\begin{aligned}(W'''(U)\tilde{u}_2\vec{\kappa}\cdot\nabla_z U, U_{z_i})_{L^2} &= \frac{\pi}{2}\kappa_i\int_0^\infty(\tilde{\mu}_2\Phi_2 + (|\vec{\kappa}|^2 - 2\eta_1 + 2\eta_2)\Phi_3)\mathcal{L}_0^2(RU')R\,dR\\ &= \frac{\pi}{2}\kappa_i\int_0^\infty\left(\tilde{\mu}_2 + \left(\frac{1}{2}|\vec{\kappa}|^2 - \eta_1 + \eta_2\right)\frac{1}{R}(RU')'\right)(RU')R\,dR\\ &= -\pi S_1\tilde{\mu}_2\kappa_i. \qquad (6.25)\end{aligned}$$

There are two terms involving only curvature-gradients of U; the first satisfies

$$\begin{aligned}(\vec{\kappa}\cdot\nabla_z((z\cdot\vec{\kappa})\vec{\kappa}\cdot\nabla_z U), U_{z_i})_2 &= -\left((z\cdot\vec{\kappa})\vec{\kappa}\cdot\nabla_z U, (\vec{\kappa}\cdot\nabla_z U)_{z_i}\right)_2\\ &= \frac{1}{2}\kappa_i\int_{\mathbb{R}^2}|\vec{\kappa}\cdot\nabla_z U|^2\,dz = \frac{\pi}{2}\kappa_i|\vec{\kappa}|^2\int_0^\infty(U')^2R\,dR = \frac{\pi}{2}S_4\kappa_i|\vec{\kappa}|^2. \qquad (6.26)\end{aligned}$$

Integrating by parts on the second term of this type yields

$$((z\cdot\vec{\kappa})\vec{\kappa}\cdot\nabla_z(\vec{\kappa}\cdot\nabla_z U), U_{z_i})_{L^2} = -\left(\vec{\kappa}\cdot\nabla_z U, |\vec{\kappa}|^2U_{z_i} + (z\cdot\vec{\kappa})(\vec{\kappa}\cdot\nabla_z U)_{z_i}\right)_{L^2},$$

where the second term on the right-hand side is evaluated as above. Expanding the first term on the right-hand side, we obtain

$$((z\cdot\vec{\kappa})\vec{\kappa}\cdot\nabla_z(\vec{\kappa}\cdot\nabla_z U), U_{z_i})_{L^2} = -\frac{\pi}{2}S_4\kappa_i|\vec{\kappa}|^2. \qquad (6.27)$$

For $i = 1, 2$, the surface diffusion terms in the solvability condition evaluate to

$$\left((\partial_s^2 + \eta_1)\vec{\kappa}\cdot\nabla_z U, U_{z_i}\right)_{L^2} = \pi S_4(\partial_s^2 + \eta_1)\kappa_i. \qquad (6.28)$$

Combining (6.22)–(6.23) with (6.25)–(6.27), the solvability condition reduces to

$$2S_1\mathbf{C}_2 - S_2\mathbf{V} = S_4\left(\partial_s^2 + \eta_1 + \frac{2S_1}{S_4}\tilde{\mu}_2 + \frac{1}{4}|\vec{\kappa}|^2\right)\vec{\kappa}, \qquad (6.29)$$

where S_1 and S_2 are as defined in (4.23) and (6.24), respectively. Since $\mu_0 = \mu_1 = 0$, the matching condition (2.43) reduces to

$$\lim_{R\to\infty}\frac{\partial\tilde{\mu}_3}{\partial R}(s, R, \theta) = \partial_{\mathbf{n}}\mu_2^{\mathbf{n}} \qquad (6.30)$$

for $\mathbf{n} = \cos\theta\,\mathbf{N}^1(s) + \sin\theta\,\mathbf{N}^2$. As in sections 4 and 5, we deduce that

$$[\partial_{\mathbf{n}}\mu_2^{\mathbf{n}}]_\Gamma = 0, \qquad (6.31)$$

$$C_{2i}(s) = \mathbf{N}^i\cdot\nabla_x\mu_2^{\mathbf{N}^i} \qquad (6.32)$$

for $i = 1, 2$, and solving (6.29) for the normal velocity yields

$$V_{2i} = \frac{2S_1}{S_2}\mathbf{N}^i\cdot\nabla_x\mu_2^{\mathbf{N}^i} - \frac{S_4}{S_2}\left(\partial_s^2 + \eta_1 + \frac{2S_1}{S_4}\tilde{\mu}_2 + \frac{3}{4}|\vec{\kappa}|^2\right)\kappa_i. \qquad (6.33)$$

6.3. Sharp-interface limit. Since the outer chemical potential solves $\Delta\mu_2 = 0$ on $\Omega\backslash\Gamma(t)$ subject to homogeneous Neumann conditions on $\partial\Omega$ and $[\partial_{\mathbf{n}}\mu_2^{\mathbf{n}}]_\Gamma = 0$, it follows from Lemma 5.3 that $\mu_2 = \mu_2(t_2)$ is a spatial constant. Consequently, $\nabla_x\mu_2 = 0$, and the normal velocity reduces to

$$\mathbf{V}_2 = -\frac{S_4}{S_2}\left(\partial_s^2 + \eta_1 + \frac{2S_1}{S_4}\mu_2 + \frac{1}{4}|\vec{\kappa}|^2\right)\vec{\kappa}. \tag{6.34}$$

As in section 5, the value of the chemical potential, μ_2, is determined through the conservation of the minority phase. Since $u_0 = b_-$ and $u_1 = 0$ in $\Omega \setminus \Gamma_\ell$, the outer chemical potential satisfies

$$\mu_2 = W''(u_0)^2 u_2 = \alpha_-^2 u_2, \tag{6.35}$$

and hence $u_2 = u_2(t_2)$ is a spatial constant. The mass of the minority phase satisfies

$$\begin{aligned} M_0 &= \int_{\Omega\setminus\Gamma_\ell} (u - b_-)\, dx + \int_{\Gamma_\ell} (\tilde{u} - b_-)\, dx \\ &= \int_\Omega (u - b_-)\, dx + \int_{\Gamma_\ell} \tilde{u} - b_- - \varepsilon^2\alpha_-^{-2}\mu_2\, dx. \end{aligned} \tag{6.36}$$

As in (5.34), we have

$$\int_\Omega (u - b_-)\, dx = \int_\Omega (\varepsilon^2 u_2 + O(\varepsilon^3))\, dx = \varepsilon^2\alpha_-^{-2}|\Omega|\mu_2 + O(\varepsilon^3). \tag{6.37}$$

For the inner integral, recalling (2.22), we have

$$\begin{aligned} \int_{\Gamma_\ell} (\tilde{u} - b_-) - \varepsilon^2\alpha_-^{-2}\mu_2\, dx &= \int_\Gamma \int_{\mathbb{R}^2} \left((\tilde{u} - b_-) - \varepsilon^2\alpha_-^{-2}\mu_2\right) J(z,s)\, dz\, ds \\ &= \int_\Gamma \int_{\mathbb{R}^2} \left(\hat{U} + \varepsilon^2(\tilde{u}_2 - \alpha_-^{-2}\mu_2)\right)(\varepsilon^2 - \varepsilon^3 z\cdot\vec{\kappa})\, dz\, ds + O(\varepsilon^5|\Gamma|) \\ &= \varepsilon^2 2\pi S_1|\Gamma| + \varepsilon^4 2\pi|\Gamma|(S_3\mu_2 + S_5|\kappa|^2) + O(\varepsilon^5|\Gamma|), \end{aligned} \tag{6.38}$$

where the $O(\varepsilon^3)$ term is zero by parity, we used (6.17) to eliminate $\tilde{u}_2$, and we introduced

$$S_5 := \int_0^\infty \Phi_3(R) R\, dR, \tag{6.39}$$

where Φ_3 is defined in (6.11) and has indefinite sign. Combining (6.37) and (6.38), the mass of the minority phase is expressed as

$$M_0 = \varepsilon^2\left(\alpha_-^{-2}|\Omega|\mu_2 + 2\pi S_1|\Gamma|\right) + \varepsilon^4|\Gamma|2\pi S_5\mu_2 + O(\varepsilon^5|\Gamma|). \tag{6.40}$$

6.3.1. Case I: $|\Gamma_0|$ is of order $O(\varepsilon^{-1})$. This scaling corresponds to Principle Result 1.1, for which $M_0 = O(\varepsilon)$. Expanding $|\Gamma|$ and M_0 as

$$|\Gamma| = \varepsilon^{-1}\gamma_{-1} + \gamma_0 + \varepsilon\gamma_1 + O(\varepsilon^2), \quad M_0 = \varepsilon\tilde{M}_0 + \varepsilon^2\tilde{M}_1 + O(\varepsilon^3), \tag{6.41}$$

the mass balance (6.40) requires

$$\tilde{M}_0 = 2\pi S_1\gamma_{-1}, \quad \tilde{M}_1 = 2\pi S_1\gamma_0 + \alpha_-^{-2}|\Omega|\mu_2. \tag{6.42}$$

Since the mass M_0 is conserved, we deduce that $\gamma_{-1} = \tilde{M}_0/(2\pi S_1)$ is independent of time, and hence $\partial_{t_2}|\Gamma| = O(\varepsilon)$.

By assumption, $\|\vec{\kappa}\|_{L^\infty(\Gamma)} = O(1)$, and from (6.34) we deduce that the normal velocity $\|\mathbf{V}_2\|_{L^\infty(\Gamma)} = O(1)$. Moreover, from (2.12) we have

$$\frac{d|\Gamma|}{dt_2} = -\int_\Gamma \vec{\kappa}\cdot\mathbf{V}_2\, ds = O(\varepsilon), \tag{6.43}$$

and from (6.34), $\mu_2(t_2)$ must satisfy

$$\mu_2 = \frac{S_4}{2S_1}\frac{\int_\Gamma |\partial_s\vec{\kappa}|^2 - \eta_1|\vec{\kappa}|^2 - \frac{1}{4}|\vec{\kappa}|^5\, ds}{\int_\Gamma |\vec{\kappa}|^2\, ds}. \tag{6.44}$$

This choice of μ_2 serves to preserve the length of Γ. Introducing the curvature-weighted projection associated to Γ, which acts on $\mathbf{F} = (f_1, f_2)^t \in L^2(\Gamma)$ as

$$\Pi_\Gamma[\mathbf{F}] := \mathbf{F} - \vec{\kappa}\frac{\int_\Gamma \mathbf{F}\cdot\vec{\kappa}\, ds}{\int_\Gamma |\vec{\kappa}|^2\, ds},$$

the normal velocity has the equivalent formulation

$$\mathbf{V}_2 = -\frac{S_4}{S_2}\Pi_\Gamma\left[\left(\partial_s^2 + \frac{1}{4}|\vec{\kappa}|^2\right)\vec{\kappa}\right], \tag{6.45}$$

where the constant η_1 drops out since $\Pi_\Gamma[\eta_1\vec{\kappa}] = 0$.

6.3.2. Case II: $|\Gamma|$ is of order $O(1)$. In this case we expand $M_0 = \varepsilon^2\tilde{M}_1 + O(\varepsilon^3)$ and $|\Gamma| = \gamma_0 + \varepsilon\gamma_1 + O(\varepsilon^2)$. The balance of terms in (6.40) yields

$$\tilde{M}_1 = 2\pi S_1\gamma_0 + \alpha_-^{-2}|\Omega|\mu_2. \tag{6.46}$$

In particular, $\gamma_0 = (\tilde{M}_1 - \alpha_-^{-2}|\Omega|\mu_2)/(2\pi S_1)$ and

$$\frac{d|\Gamma|}{dt_2} = -\frac{|\Omega|\mu_2'(t_2)}{2\pi S_1\alpha_-^2} + O(\varepsilon). \tag{6.47}$$

From (6.34), the leading order terms yield the coupled system

$$\mu_2'(t_2) = 2\pi S_1\alpha_-^2|\Omega|^{-1}\int_\Gamma \mathbf{V}\cdot\vec{\kappa}\, ds, \tag{6.48}$$

$$\mathbf{V} = -\frac{S_4}{S_2}\left(\partial_s^2 + \eta_1 + \frac{2S_1}{S_4}\mu_2 + \frac{1}{4}|\vec{\kappa}|^2\right)\vec{\kappa}. \tag{6.49}$$

7. Competitive geometric flows. In an amphiphilic system it is possible for bilayers and pore structures to coexist on the slow time scale and compete with one another for the surfactant phase. Indeed, consider the pore profile, $U = U_p$, constructed in (3.9), and the bilayer profile, U_b, which is the homoclinic solution of

$$\partial_r^2 U_b = W'(U_b), \tag{7.1}$$

subject to the condition $U_b \to b_-$ as $r \to \pm\infty$. We have shown that for any closed codimension two manifold, $\Gamma_p \subset \Omega \subset \mathbb{R}^3$, we may associate a pore solution of the form

$$u(x,t) = U_p(z_1, z_2) + \varepsilon^2 u_{2p}(x,t) + O(\varepsilon^3), \tag{7.2}$$

where $u_{2p}(x,t) \to \mu_2\alpha_-^{-2}$ at an $O(1)$ exponential rate in the *ε-scaled* distance, $|(z_1,z_2)|$, to Γ_p. Here $\mu_2 = \mu_2(t_2)$ is the spatially constant, time dependent value of the outer chemical potential. Similarly, in [10] we showed that for any codimension one hypersurface, $\Gamma_b \subset \Omega \subset \mathbb{R}^3$, we may associate a bilayer solution of the form

$$u(x,t) = U_b(r) + \varepsilon^2 u_{2b}(x,t) + O(\varepsilon^3), \tag{7.3}$$

where U_b is the homoclinic solution of (7.1) and $u_{2b}(x,t) \to \mu_2\alpha_-^{-2}$ at an $O(1)$ exponential rate in the *ε-scaled* signed distance, r, to Γ_b. It is trivial to extend this construction to coexisting bilayer and pore structures, with a common value of the outer chemical potential μ_2, so long as the submanifolds are uniformly smooth and are an $O(1)$ distance from both self-intersection and intersection with each other. Indeed, the composite solution takes the form

$$u(x,t) = U_p(z_1,z_2) + U_b(r) + \varepsilon^2\left(u_{2p}(x,t) + u_{2b}(x,t) - \frac{\mu_2}{\alpha_-^2}\right) + O(\varepsilon^3), \tag{7.4}$$

where the two morphologies, characterized by the disjoint codimension one and two manifolds Γ_b and Γ_p, compete with each other for surfactant phase through the common, temporally varying, value of $\mu_2 = \mu_2(t_2)$.

The normal velocities of the bilayer and pore morphologies are given by (1.13) and (1.15), coupled through the outer chemical potential μ_2. The evolution of the outer chemical potential is determined by the mass constraint for the combined bilayer-pore structures. For u, a combined bilayer-pore solution of the form (7.4), conservation of mass implies that

$$\begin{aligned} M &:= \int_\Omega (u_0 - b_-)\,dx = \int_\Omega (u(x,t) - b_-)\,dx \\ &= \int_{\Gamma_{b,\ell}} \hat{U}_b(r(x))\,dx + \int_{\Gamma_{p,\ell}} \hat{U}_p(z(x))\,dx + O\big(\varepsilon^2|\Gamma_p|, \varepsilon^2|\Gamma_b|\big)\,, \end{aligned} \tag{7.5}$$

where $\Gamma_{b,\ell}$ and $\Gamma_{p,\ell}$ are the regions of Ω whose points are within $\varepsilon\ell$ of Γ_b and Γ_p, respectively. The shifted bilayer $\hat{U}_b := U_b - b_-$ and shifted pore profile $\hat{U}_p := U_p - b_-$ reflect the amphiphilic mass above the base line b_-, in terms of the bilayer and pore profiles defined in (1.7) and (1.8). A small total mass $M = \varepsilon M_0 + O(\varepsilon^2)$ requires that $|\Gamma_b| = O(1)$ and $|\Gamma_p| = O(\varepsilon^{-1})$. Changing to local variables in the mass constraint integrals yields the leading-order identity

$$m_b|\Gamma_b| + m_p\varepsilon|\Gamma_p| = M_0, \tag{7.6}$$

where m_b and m_p are as introduced in (1.14) and Principle Result 1.1. Equivalently, taking the time derivative, we have

$$m_b\frac{d}{dt}|\Gamma_b| + m_p\varepsilon\frac{d}{dt}|\Gamma_p| = 0. \tag{7.7}$$

From (2.12) and the bilayer equivalent

$$\frac{d|\Gamma_b|}{dt} = \int_{\Gamma_b} V_b H\,dS,$$

the normal velocity expressions (1.13) and (1.15) yield leading-order expressions for change in bilayer surface area and pore length,

$$\frac{d|\Gamma_b|}{dt} = \frac{\sigma_b}{m_b}\int_{\Gamma_b}\left[\left(K - \frac{H^2}{2} + \frac{\eta_1+\eta_2}{2} + \lambda_b\mu_2\right)H^2 - |\nabla_s H|^2\right]dS, \tag{7.8}$$

$$\frac{d|\Gamma_p|}{dt} = \frac{\sigma_p}{m_p}\int_{\Gamma_p}\left[\left(\frac{1}{4}|\vec{\kappa}|^2 + \eta_1 + \lambda_p\mu_2\right)|\vec{\kappa}|^2 - |\partial_s\vec{\kappa}|^2\right] ds. \tag{7.9}$$

Since only an $O(\varepsilon^2)$ quantity of surfactant is contained in the outer region, away from the pores and bilayers, the total mass contained in the bilayer and pores is effectively conserved, and any increase in bilayer surface area will result in a decrease of net pore length, and vice versa. Moreover, the overall evolution is sensitive not only to the particular geometric configuration, that is, the curvatures of Γ_p and Γ_b, but also to the well-shape, through λ_b and λ_p, and the parameter η_1. The mass constraint (7.7) determines the evolution of $\mu_2(t_2)$ through the relations (7.8), and (7.9), which yield a closed, coupled system for the curvature driven flows (1.13) and (1.15). While the overall system is nontrivial to resolve in a general framework, the interaction laws of geometrically simple structures can be explicitly determined.

7.1. Competition among spherical bilayers and circular pores. Collections of spatially well-separated, spherically symmetric bilayers and closed, circular pores form an approximately invariant manifold of (1.12), up to exponentially small terms associated to tail-tail interactions, which are beyond our analysis. While there are rigorous methods to establish the existence of fully invariant manifolds in neighborhoods of approximately invariant ones (see [2]), in the spirit of our formal analysis we merely recover the leading-order dynamics. To this end, at time t we suppose there are $N_b \in \mathbb{N}_+$ spherical bilayer structures with radii $R_i(t)$ for $i = 1, \dots, N_b$ and $N_p \in \mathbb{N}_+$ closed, circular pores of radii $r_i(t)$ for $i = 1, \dots, N_p$; see Figure 1. To be consistent with a total surfactant phase which is $O(\varepsilon)$, we assume that each radius is $O(1)$, and $N_b = O(1)$ while $N_p = O(\varepsilon^{-1})$. Since the curvatures of the bilayers and pores are independent of position along these interfaces, the surface derivative terms in (7.8) and (7.9) are zero. In addition, in (7.8) the higher-order curvature term $K - \frac{1}{2}H^2$ is zero for a sphere in $\mathbb{R}^3$. Since the ith spherical bilayer has center-line surface area $4\pi R_i^2$, while the ith closed pore has center-line length $2\pi r_i$, we may apply (7.8) and (7.9) individually to each distinct structure, rewriting the equations as a coupled system of ordinary differential equations for the evolution of the radii,

$$\dot{R}_i = \frac{2\sigma_b}{m_b}\left(\frac{\eta_1+\eta_2}{2} + \lambda_b\mu_2\right)\frac{1}{R_i}, \quad i = 1, \dots, N_b, \tag{7.10}$$

$$\dot{r}_j = \frac{\sigma_p}{m_p}\left(\frac{1}{4r_j^2} + \eta_1 + \lambda_p\mu_2\right)\frac{1}{r_j}, \quad j = 1, \dots, N_p. \tag{7.11}$$

The coupling is through the common, background value, $\mu_2 = \mu_2(t_2)$, of the chemical potential. Its value is determined through the conservation of mass relation, (7.7), which balances the volumes of surfactant phase in each family of structures. Simplifying this relation, we determine

$$\mu_2(\vec{r}) = -\frac{\left(4N_b\sigma_b + \varepsilon\sigma_p\sum_{j=1}^{N_p} r_j^{-1}\right)\eta_1 + 4N_b\sigma_b\eta_2 + \frac{1}{4}\varepsilon\sigma_p\sum_{j=1}^{N_p} r_j^{-3}}{8N_b\sigma_b\lambda_b + \varepsilon\sigma_p\lambda_p\sum_{j=1}^{N_p} r_j^{-1}}. \tag{7.12}$$

The mean field μ_2 depends upon the particular values of the circular pore radii, $\vec{r} := (r_1, \dots, r_{N_p})^t$; however, it is independent of the bilayer radii, $\vec{R} := (R_1, \dots, R_{N_b})^t$, depending only upon their total number, N_b. So long as N_b is constant, the system is

upper-triangular, with the pore evolution forming a closed system, while the bilayer evolution depends upon the evolution of the pores.

The equilibria form an overconstrained system, with $N_p + 1$ equations for the N_p pore radii, $\vec{r}$. From the form of (7.11) and (7.12), the pore radii take a common equilibria value

$$r_{\rm eq} := \sqrt{\frac{\lambda_b}{2\left((\lambda_p - 2\lambda_b)\eta_1 + \lambda_p\eta_2\right)}}, \tag{7.13}$$

and evaluating the chemical potential at $\vec{r}_{\rm eq} := (r_{\rm eq}, \ldots, r_{\rm eq})^T$, one obtains

$$\mu_2(\vec{r}_{\rm eq}) = -\frac{\eta_1 + \eta_2}{2\lambda_b}, \tag{7.14}$$

which, quite remarkably, coincides with the equilibrium value of μ_2 for the bilayer radii. This coincidence renders the overdetermined system solvable, with the impact that there are large families of equilibrium configurations. Indeed, so long as the bifurcation parameter

$$\nu := (\lambda_p - 2\lambda_b)\eta_1 + \lambda_p\eta_2$$

is positive, there exist equilibria consisting of N_p circular pores with common radius $r_{\rm eq}$ coexisting with N_b spherical bilayers of arbitrary radii, $\vec{R} \in \mathbb{R}_+^{N_b}$.

While the full dynamics of (7.10)–(7.12) are nontrivial, several important properties of the system can be readily extracted. In particular, the spherical bilayers either all grow, if $\mu_2 > -(\eta_1 + \eta_2)/(2\lambda_b)$, or all shrink, if $\mu_2 < -(\eta_1 + \eta_2)/(2\lambda_b)$. Moreover, when $\nu < 0$, not only do the circular pores and spherical bilayers fail to coexist, but the spherical bilayers must shrink until they reach an $O(\varepsilon)$ radius. Indeed, substituting (7.12) into (7.10) and simplifying, we obtain the form

$$\dot{R}_i = \frac{1}{R_i}\frac{\varepsilon\sigma_b\sigma_p}{m_b}\frac{\nu\sum\limits_{j=1}^{N_p} r_j^{-1} - \frac{1}{2}\lambda_b\sum\limits_{j=1}^{N_p} r_j^{-3}}{8N_b\sigma_b\lambda_b + \varepsilon\sigma_p\lambda_p\sum\limits_{j=1}^{N_p} r_j^{-1}}, \tag{7.15}$$

which confirms that $\dot{R}_i < 0$ when $\nu < 0$. Since the radii $\vec{r}$ of the circular pores are bounded above by mass constraints, the spherical bilayers must shrink with a uniform rate, individually reaching an $O(\varepsilon)$ radius in an $O(1)$ time on the t_2 time scale. At this point the interface underlying the spherical bilayer is not far from self-intersection, and the analysis leading to (7.10) is no longer valid. We conjecture that such a sufficiently small spherical bilayer will extinguish, at which instant N_b decreases by one. Although, it is also plausible that a small radius bilayer may break up into a family of micelles or form a closed-loop pore or other solution of (1.4).

On the other hand, for $\nu > 0$, the equilibrium configurations composed of N_b spherical bilayers coexisting with N_p circular pores of common radius $r_{\rm eq}$ are asymptotically stable to perturbations in the radii. Indeed, since $\dot{R}_i$ is small near the equilibria, we may assume that N_b is constant; the nonlinear asymptotic stability of the family then follows from the linear stability of $\vec{r} = \vec{r}_{\rm eq}$ within the closed evolution for the circular pore radii. We write this system in the form

$$\frac{d\vec{r}}{dt} = F(\vec{r}; N_b), \tag{7.16}$$

where F depends upon $\mu_2 = \mu_2(\vec{r}; N_b)$. We must determine the eigenvalues of the $N_p \times N_p$ matrix $\nabla_{\vec{r}} F(\vec{r}_{\rm eq})$. We introduce the quantity $\tilde{\mu}_2(r) := \mu_2(r, \dots, r)$, which satisfies

$$\tilde{\mu}_2 = -\frac{4\sigma_b N_b(\eta_1+\eta_2) + \varepsilon\sigma_p N_p(\eta_1 r^{-1} + \frac{1}{4}r^{-3})}{8\sigma_b N_b\lambda_b + \varepsilon\sigma_p N_p\lambda_p r^{-1}}. \tag{7.17}$$

Taking the gradient of (7.11) and using the relation (7.14), we calculate that

$$\nabla_{\vec{r}} F(\vec{r}_{\rm eq}) = \frac{\sigma_p}{m_p}\left(-\frac{1}{2r_{\rm eq}^4}\mathbf{I} + \frac{\lambda_p\tilde{\mu}_2'(r_{\rm eq})}{r_{\rm eq}}\mathbf{O}\right),$$

where $\mathbf{O}$ denotes the $N_p \times N_p$ matrix, all of whose entries are one, and $\mathbf{I}$ denotes the $N_p \times N_p$ identity matrix.

The matrix $\nabla_{\vec{r}} F(\vec{r}_{\rm eq})$ has an $N_p - 1$ dimensional eigenspace, given by $\ker(\mathbf{O})$, associated to the eigenvalue $\lambda_0 = -\sigma_p/(2m_p r_{\rm eq}^4) < 0$. This eigenvalue and eigenspace establish the stability to perturbations which break the equality of the circular pore radii. The remaining eigenspace is spanned by the vector $(1, \dots, 1)^t$ and has eigenvalue

$$\begin{aligned}\lambda_1 &= \frac{\sigma_p}{m_p}\left(-\frac{1}{2r_{\rm eq}^4} + \frac{N_p\lambda_p\tilde{\mu}_2'(r_{\rm eq})}{r_{\rm eq}}\right)\\ &= -\frac{\sigma_p}{m_p r_{\rm eq}^4}\left(\frac{1}{2} + \frac{\varepsilon\sigma_p N_p^2\lambda_p^2}{4(8\sigma_b N_b\lambda_b + \varepsilon\sigma_p N_p\lambda_p r_{\rm eq}^{-1})}\right).\end{aligned}$$

Since $\lambda_1 < 0$, this establishes the linear, and hence nonlinear, asymptotic stability of the mixed equilibria to radial perturbations, and confirms the final statement of Principle Result 1.2.

Remark 7.1. In the absence of bilayers, when $N_b = 0$, then η_1 and η_2 drop out of the pore evolution equation, which reduces to

$$\dot{r}_j = \frac{\pi\sigma_p}{2m_p}\left(\frac{1}{r_j^2} - \frac{\sum_{j=1}^{N_p} r_j^{-3}}{\sum_{j=1}^{N_p} r_j^{-1}}\right). \tag{7.18}$$

Any common value of the circular pore radii, $\vec{r} = (r, \dots, r)^t$, is a stable equilibrium. However, adding a single spherical bilayer, in the $\nu > 0$ regime, will drive the pores to their equilibrium radius, $r_{\rm eq}$, assuming the bilayer persists.

REFERENCES

[1] O. Andreussi, I. Dabo, and N. Marzari, *Revised self-consistent continuum solvation in electronic-structure calculations*, J. Chem. Phys., 136 (2012), 064102.

[2] P. Bates, K. Lu, and C. Zeng, *Approximately invariant manifolds and global dynamics of spike states*, Invent. Math., 174 (2008), pp. 355–433.

[3] I. Budin and J. Szostak, *Physical effects underlying the transition from primitive to modern cell membranes*, Proc. Natl. Acad. Sci. USA, 108 (2011), pp. 5249–5254.

[4] J. W. Cahn and J. E. Hilliard, *Free energy of a nonuniform system* I. *Interfacial energy*, J. Chem. Phys., 28 (1958), pp. 258–267.

[5] A. Calini and T. Ivey, *Stability of small-amplitude torus knot solutions of the localized induction approximation*, J. Phys. A, 44 (2011), 335204.

[6] F. Campelo and A. Hernández-Machado, *Model of curvature-driven pearling instability in membranes*, Phys. Rev. Lett., 99 (2007), 088101.

[7] P. Canham, *Minimum energy of bending as a possible explanation of biconcave shape of human red blood cell*, J. Theoret. Biol., 26 (1970), pp. 61–81.

[8] S. Cox and P. Matthews, *Exponential time differencing for stiff systems*, J. Comput. Phys., 176 (2002), pp. 430–455.
[9] S. Dai and Q. Du, *Motion of interfaces governed by the Cahn–Hilliard equation with highly disparate diffusion mobility*, SIAM J. Appl. Math., 72 (2012), pp. 1818–1841.
[10] S. Dai and K. Promislow, *Geometric evolution of bilayers under the functionalized Cahn-Hilliard equation*, Proc. R. Soc. Lond. Ser. A Math. Phys. Eng. Sci., 469 (2013), 20120505.
[11] A. Doelman, G. Hayrapetyan, K. Promislow, and B. Wetton, *Meander and pearling of single-curvature bilayer interfaces in the functionalized Cahn–Hilliard equation*, SIAM J. Math. Anal., 46 (2014), pp. 3640–3677.
[12] G. Hayrapetyan and K. Promislow, *Nonlinear stability and meander of bilayers under the weak Functionalized Cahn-Hilliard flow*, preprint.
[13] Q. Du, C. Liu, and X. Wang, *Simulating the deformation of vesicle membranes under elastic bending energy in three dimensions*, J. Comput. Phys., 212 (2006), pp. 757–777.
[14] L. C. Evans, *Partial Differential Equations*, Grad. Stud. Math. 19, AMS, Providence, RI, 1998.
[15] F. Lin and X. Yang, *Geometric Measure Theory: An Introduction*, Advanced Mathematics 1, International Press, Boston, MA, 2002.
[16] N. Gavish, G. Hayrapetyan, K. Promislow, and L. Yang, *Curvature driven flow of bilayer interfaces*, Phys. D, 240 (2011), pp. 675–693.
[17] N. Gavish, J. Jones, Z. Xu, A. Christlieb, and K. Promislow, *Variational models of network formation and ion transport: Applications to perfluorosulfonate ionomer membranes*, Polymers, 4 (2012), pp. 630–655.
[18] G. Gompper and M. Schick, *Correlation between structural and interfacial properties of amphiphilic systems*, Phys. Rev. Lett., 65 (1990), pp. 1116–1119.
[19] G. M. Grason and C. D. Santangelo, *Undulated cylinders of charged diblock copolymers*, European Phys. J. E, 20 (2006), pp. 335–346.
[20] G. Hayrapetyan and K. Promislow, *Spectra of functionalized operators arising from hypersurfaces*, Z. Angew. Math. Phys., DOI 10.1007/s00033-014-0443-42014, 2014.
[21] W. Helfrich, *Elastic properties of lipid bilayers—theory and possible experiments*, Z. Naturforschung C, 28 (1973), pp. 693–703.
[22] W. Hsu and T. Gierke, *Ion transport and clustering in Nafion perfluorinated membranes*, J. Membrane Sci., 13 (1983), pp. 307–326.
[23] S. Jain and F. Bates, *On the origins of morphological complexity in block copolymer surfactants*, Science, 300 (2003), pp. 460–464.
[24] S. Jain and F. Bates, *Consequences of nonergodicity in aqueous binary PEO-PB micellar dispersions*, Macromolecules, 37 (2004), pp. 1511–1523.
[25] T. Kapitula and K. Promislow, *Spectral and Dynamical Stability of Nonlinear Waves*, Springer, New York, 2013.
[26] C. Knox and G. Voth, *Probing selected morphological models of hydrated Nafion using large-scale molecular dynamics simulations*, J. Phys. Chem. B, 144 (2010), pp. 3205–3218.
[27] P. Loreti and R. March, *Propagation of fronts in a nonlinear fourth order equation*, Euro. J. Appl. Math., 11 (2000), pp. 203–213.
[28] J. Lowengrub, A. Ratz, and A. Voigt, *Phase-field modeling of the dynamics of multicomponent vesicles: Spinodal decomposition, coarsening, budding, and fission*, Phys. Rev. E, 79 (2009), 031925-1:13.
[29] R. L. Pego, *Front migration in the nonlinear Cahn-Hilliard equation*, Proc. Roy. Soc. London Ser. A, 442 (1989), pp. 261–278.
[30] J. Polking, *A Survey of Removable Singularities*, Springer-Verlag, New York, 1988.
[31] K. Promislow and H. Zhang, *Critical points of functionalized Lagrangians*, Discrete Contin. Dyn. Syst. Ser. A, 33 (2013), pp. 1–16.
[32] M. Röger and R. Schätzle, *On a modified conjecture of De Giorgi*, Math. Z., 254 (2006), pp. 675–714.
[33] L. Rubatat, A. L. Rollet, G. Gebel, and O. Diat, *Evidence of elongated polymeric aggregates in Nafion*, Macromolecules, 35 (2002), pp. 4050–4055.
[34] L. Rubatat, G. Gebel, and O. Diat, *Fibriallar structure of Nafion: Matching Fourier and real space studies of corresponding films and solutions*, Macromolecules, 37 (2004), pp. 7772–7783.
[35] D. A. Scherlis, J. L. Fattebert, F. Gygi, M. Cococcioni, and N. Marzari, *A unified electrostatic and cavitation model for first-principles molecular dynamics in solution*, J. Chem. Phys., 124 (2006), 074103.
[36] K. Schmidt-Rohr and Q. Chen, *Parallel cylindrical water nanochannels in Nafion fuel cell membranes*, Nature Materials, 7 (2008), pp. 75–83.

[37] M. Teubner and R. Strey, *Origin of scattering peaks in microemulsions*, J. Chem. Phys., 87 (1987), pp. 3195–3200.

[38] S. Torabi, J. Lowengrub, A. Voigt, and S. Wise, *A new phase-field model for strongly anisotropic systems*, Proc. R. Soc. Lond. Ser. A Math. Phys. Eng. Sci., 465 (2009), pp. 1337–1359.

[39] J. Zhu and R. Hayward, *Wormlike micelles with microphase-separated cores from blends of amphiphilic AB and hydrophobic BC diblock copolymers*, Macromolecules, 41 (2008), pp. 7794–7797.

[40] J. Zhu, N. Ferrer, and R. Hayward, *Tuning the assembly of amphiphilic block copolymers through instabilities of solvent/water interfaces in the presence of aqueous surfactants*, Soft Matter, 5 (2009) pp. 2471–2478.

[41] J. Zhu and R. Hayward, *Interfacial tension of evaporating emulsion droplets containing amphiphilic block copolymers: Effects of solvent and polymer composition*, J. Colloid Interfacial Sci., 365 (2012), pp. 275–279.